



mekanika

Mechanical Engineering Scientific Magazine

Fama Aqiftiar Falah, Suyitno, Syamsul Hadi

The Manufacturing of Thermal Conductivity Testing Apparatus

Widhaya Bastian Purnama, Indri Yaningsih, Heru Sukanto

The Utilizing Cutting Fluid And Feeding Rate Effect to The Surface Hardness And Precission of Aluminum Material Using CNC Milling Machine

Achmad Gustiantono, Dominicus Danardono Dwi Prija Tjahjana, Syamsul Hadi

Wind Turbine Vertical Axis H Rotor Type with 1 Kw Capacity at Suwuk Beach, Kebumen

Antonius Adi Hendra Saputra, Joko Triyono, Teguh Triyono

Bovine Bone Hidroksiapatite Materials Mechanics Properties at 900°C and 1200°C of Calcination Temperature

Fajar Paundra, Teguh Triyono, Wahyu Purwo

Cu Addition Effect Analysis on Matrix of Remelting Piston Aluminium Composite with Silica Sand Reinsforcement to The Impact Strength and Micro Structure on Aluminuim Matrix Composite Using Stir-Casting Method

Gilang Sigit Saputro, Triyono, Nurul Muhayat

Welding Current and Shielding Gas Flow Rate Effect to The Intermetallic Layer Formation of Tungsten Inert Gas (TIG) on Dissimilar Metals Weld Joints Between Galvanized Steel and Aluminium AA 5052 By Using Al-Si 4043 Filler

MEKANIKA

Volume 16

Number 1

Page
1-36

Surakarta
March 2017

ISSN: 1412-7962
e-ISSN: 2579-3144

Mechanical Engineering Department Faculty of Engineering
Universitas Sebelas Maret

mekanika

Mechanical Engineering Scientific Magazine

EDITORIAL BOARD

Chancellor

Head of Mechanical Engineering Department
Dr. Eng. Syamsul Hadi, ST, MT

Managing Editor

Indri Yaningsih, ST, MT

Co-Managing Editor

Wibawa Endra Juwana, ST, MT

Associate Editor

Prof. Dr. Kuncoro Dihadjo, ST, MT
Prof. Dr. Muhammad Nizam, ST, MT
Prof. Dr. Dwi Aries Himawanto, ST, MT
Prof. Dr. techn. Suyitno, ST, MT
Ir. Agung Tri Wijayanta, ST, M.Sc, Ph.D
Dr. Budi Santoso, ST,MT
Dr. Budi Kristiawan, ST, MT
D. Danardono, DPT, ST, MT, Ph.D
Dr. Triyono, ST, MT
Dr. Joko Triyono, ST, MT
Dr. Eko Surojo, ST, MT
Dr. Nurul Muhayat, ST, MT
Ir. Ubaidillah, ST, M.Sc., Ph.D
Dr. Zainal Arifin, ST, MT
Prof. Ir. Dr. Saiful Amri Mazlan
Fitrian Imaduddin, ST, M.Sc, Ph.D

Editor of the Implementer

Sukmaji Indro Cahyono, ST, M.Eng

Editorial Assistance

Ariyo Nurachman Satiya Permata, ST

Editorial Address

Mechanical Engineering Department Faculty of Engineering
Universitas Sebelas Maret

Jalan Ir. Sutami 36A Surakarta 57126

Telp. (0271) 632163

Fax. (0271) 662118

Website <http://jurnal.ft.uns.ac.id/index.php/mekanika>

E-mail : mekanika_jtmuns@yahoo.com

Editors invite Academician, Researcher, Practitioner, and Professional to contribute an article in mechanical engineering field which is a research or literature review that have not been published on other media. It is issued twice time in a year which are in March and September. The manuscript has been accepted by editorial not more than two months before the publication. It is preferred to post it via e-mail.

mekanika

Mechanical Engineering Scientific Magazine

ISSN 1412 – 7962, Volume 16 Number 1, March 2017

The Manufacturing of Thermal Conductivity Testing Apparatus Fama Aqiftiar Falah, Suyitno, Syamsul Hadi	1-6
The Utilizing Cutting Fluid And Feeding Rate Effect to The Surface Hardness And Precission of Aluminum Material Using CNC Milling Machine Widhaya Bastian Purnama, Indri Yaningsih, Heru Sukanto	7-13
Wind Turbine Vertical Axis H Rotor Type with 1 Kw Capacity at Suwuk Beach, Kebumen Achmad Gustiantono, Dominicus DDPT, Syamsul Hadi	14-18
Bovine Bone Hidroksiapatite Materials Mechanics Properties at 900°C and 1200°C of Calcination Temperature Antonius Adi Hendra Saputra, Joko Triyono, Teguh Triyono	19-23
Cu Addition Effect Analysis on Matrix of Remelting Piston Aluminium Composite with Silica Sand Reinsforcement to The Impact Strength and Micro Structure on Aluminuim Matrix Composite Using Stir-Casting Method Fajar Paundra, Teguh Triyono, Wahyu Purwo Raharjo	24-29
Welding Current and Shielding Gas Flow Rate Effect to The Intermetallic Layer Formation of Tungsten Inert Gas (TIG) on Dissimilar Metals Weld Joints Between Galvanized Steel and Aluminium AA 5052 By Using Al-Si 4043 Filler Gilang Sigit Saputro, Triyono, Nurul Muhayat	30-36

PREFACE

Syukur Alhamdulillah, for mercy and guidance from Allah SWT, Mechanical Engineering Scientific Magazine Volume 16 Number 1, March 2017 has been issued. Editorial boards want to say many thanks to contributors and associate editor who have provided contributions on its quality.

In this edition, journal displays 11 articles of University which represent 4 (four) of each discipline, Energy Conversion, Material/ Metallurgy and Manufacture, and Design. It begins by Fama Aqiftiar Falah et al with the title **“The Manufacturing of Thermal Conductivity Testing Apparatus”**, Widhaya Bastian Purnama et al with the title **“The Utilizing Cutting Fluid And Feeding Rate Effect to The Surface Hardness And Precission of Aluminum Material Using CNC Milling Machine”**, Achmad Gustiantono et al with the title **“Wind Turbine Vertical Axis H Rotor Type with 1 Kw Capacity at Suwuk Beach, Kebumen”**, Antonius Adi Hendra Saputra et al with the title **“Bovine Bone Hidroksiapatite Materials Mechanics Properties at 900°C and 1200°C of Calcination Temperature”**, Fajar Paundra et al with the title **“Cu Addition Effect Analysis on Matrix of Remelting Piston Aluminium Composite with Silica Sand Reinsforcement to The Impact Strength and Micro Structure on Aluminuim Matrix Composite Using Stir-Casting Method”**, Gilang Sigit Saputro et al with the title **“Welding Current and Shielding Gas Flow Rate Effect to The Intermetallic Layer Formation of Tungsten Inert Gas (TIG) on Dissimilar Metals Weld Joints Between Galvanized Steel and Aluminium AA 5052 By Using Al-Si 4043 Filler”**.

We invite academician, researcher, practitioner, and professional to contribute an article in mechanical engineering field at mechanical engineering scientific magazine, which issues in March and September. Finally, we wish that these articles can be beneficially for readers, be accessible information exchange media of research result, and allocate inspiration on technology development especially mechanical engineering.

Editorial Board

THE MANUFACTURING OF THERMAL CONDUCTIVITY TESTING APPARATUS

Fama Aqiftiar Falah¹, Suyitno², Syamsul Hadi²

¹Mahasiswa Program Sarjana Jurusan Teknik Mesin – Universitas Sebelas Maret

²Staf Pengajar – Jurusan Teknik Mesin – Universitas Sebelas Maret

e-mail addresses: fama.aqiftiar@gmail.com (Fama AF.), suyitno@gmail.com (Suyitno)
syamsulh_st@yahoo.com (Syamsul H.)

Keywords:

Thermal conductivity, steady-state, axial heat transfer, high temperature

Abstract

This study presents the designing and constructing process of thermal conductivity apparatus using steady-state heat-transfer techniques with the capability to test the material at high temperatures. The design of apparatus is an improvement of ASTM D5470 standard where meter-bar with the equal cross-sectional area with used to extrapolate surface temperature and heat transfer across a sample under test. There were two meter-bars in apparatus testing, where every meter-bar were placed 3 thermocouples. The test apparatus used a heater with a power of 1.000 Watt, and a water cooler in order to keep the temperature stable. The pressure applied to specimens was 3.4 MPa at cross-sectional area 113,09 mm² meter-bar and thermal grease minimized interfacial thermal resistance. To determine the performance of this apparatus, validating process was proceed by comparing the results with thermal conductivity apparatus obtained by THB 500 made by LINSEIS. The tests showed the value of the thermal conductivity of the stainless steel and bronze is 15,28 Wm⁻¹K⁻¹ and 38,01 Wm⁻¹K⁻¹ with a difference of test apparatus THB 500 were -2,55% and 2,49%. For high temperature this apparatus is able to reach the testing temperature of 400°C for test results of stainless steel with 19,21 Wm⁻¹K⁻¹ difference of 7,93% from the literature.

PENDAHULUAN

The thermal conductivity is one of the basic properties of the material, ie the rate of heat transfer through a unit thickness of material per unit area per a temperature gradient [1]. The thermal conductivity can also show how fast heat flows in specific materials [2]. High thermal conductivity value which indicates that the material is a conductor, while its low thermal conductivity of the material is an insulator [1].

Another thing, the thermal conductivity value of a particular material can vary depending on the content of the material. Other than that, environmental conditions also affect the value of the thermal conductivity of the material, one of which is the temperature of the environment [3]. Variations of thermal conductivity at a certain temperature range was ignored for some material, but significant for the particular material. The temperature effect on the thermal conductivity values cause analysis on heat transfer conduction becomes complicated. Therefore, the thermal conductivity calculation was assumed to have a constant value which was determined from the average temperature [1]. However, for thermoelectric materials which operate at high temperatures, for example in the thermoelectric (ZnO semiconductor doping Cu) that operates at a temperature of 450°C [4] needed an apparatus that is testing capability at the operating temperature to get more accurate results.

Generally, the thermal conductivity testing can be classified into two main categories, namely: (1) steady state and (2) transient, some of which can be either absolute or comparative methods. As the name implies testing (1) depending on the steady state temperature gradient, (2) the dynamic temperature state. As the dynamic temperature field, transient testing method was also able to produce other than thermal conductivity properties, which were the specific heat and thermal diffusivity. Apart from these two main categories, there were also 3 ω testing methods which employed to the thermal conductivity test of thin films [5, 6]

For a relatively large sample may be used technique of steady-state and nanoequilibrium, however for a small sample will be difficult. Commercial methods most widely used to the thermoelectric material test was laser flash method diffusivity transient technique, but this method required some more testing device to determine the thermal conductivity. Besides from that, this method has its limitations for materials with high thermal conductivity and high temperature [7]. The thermal conductivity testing at high temperature axial heat flow method was used by the standard ASTM E 1225 with the planting of a thermocouple on the specimen to determine the thermal conductivity of the testing material [6, 8]. However, it can not be done on thermo electric material which is thin and

fragile material properties when machining process was executing.

In this research will be designed and manufactured thermal conductivity test tool with axial heat flow method approach to heat flow in steady state with a thin material and without planting a thermocouple in the test sample. Furthermore, this test validated using stainless steel material and Bronze. The temperature data is monitored and processed using ADAM 4018 as a data acquisition tool. In addition, this test will be made to test the thermoelectric material with a testing temperature of 400 ° C.

RESEARCH METHODS

This study was a research about design which was experimentally performed to obtain the best performance of testing equipment. It was made from ASTM D5470 standard reference which using the one-dimensional steady state conduction techniques. The explanation can be clearly seen in Figure 1 and Figure 2.

Testing Equipment Design

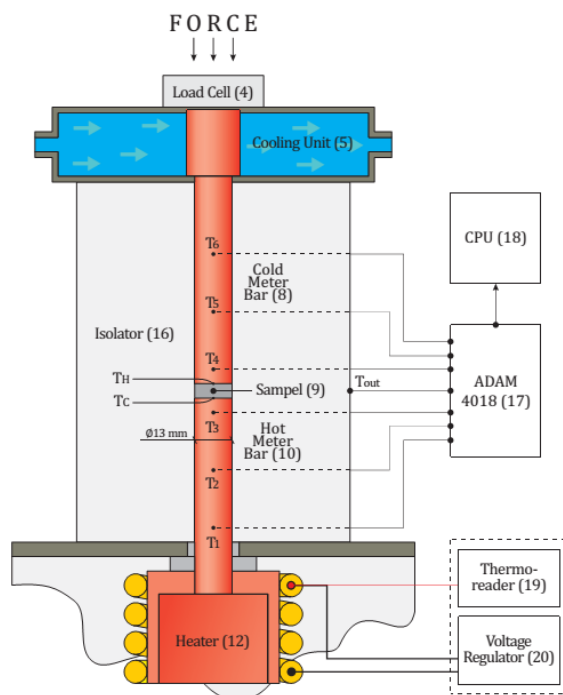


Figure 1. Thermal conductivity testing scheme based on ASTM D5470 standard. (17) ADAM 4018 (18) CPU (19) Thermo-reader (20) Voltage regulator

The testing equipment framework was consisted of top base plate (2), middle base plate (6), bottom base plate (14) which made of mildsteel with 300×180×5mm of size, and vertical rod (3) which fabricated of stainless steel with 500 mm of height and 20 mm of diameter. At the top, there was a lever base plate (1) which applied pressure to the sample during the test. It pressed the load cell (4) was then passed to the middle base plate which can be moved up and down using a linear bearing (7) was sliding

by a vertical rod. At the bottom, there was a middle base plate cooling unit (5) which cools the cold meter bar (8). Cooling water was circulated using a pump to maintain a flow and current of water at the system in steady state. At the bottom of the base plate was placed set heater (12) and putted an insulator to separate them (13) which was aimed to keep the temperature at the bottom base plate normally. The testing equipment was designed to have a high operating capability at 400°C of temperature, using 1250 Watt of heater element to heat a hot meter bar (10) until it reached that temperature. The heater was located at bottom and controlled using a voltage regulator (20) with output current and voltage to provide power to the heater. The heater temperature was controlled using a thermo-reader (19) which was placed on the panel box. Between the cold meter bar and hot meter bar was placed specimens (9) with 13 mm of diameter. At each meter bar there were 3 thermocouple (11) which used to read the temperature gradients that occurred away from the hot meter bar to the cold meter bar. Meter bar and specimen were covered with an insulator (16) to keep the system in order to adiabatic. At the time of the test applied, 0.069 MPa and 3.4 MPa of pressure for soft materials to hard materials respectively, 113.09 mm² of meter bar cross-sectional area. Thermocouple that used was the K type due to its high temperatures resistant. Data from the thermocouple was read employing Analog to Digital Converter Advantech ADAM 4018 (17) and forwarded to a computer (18).

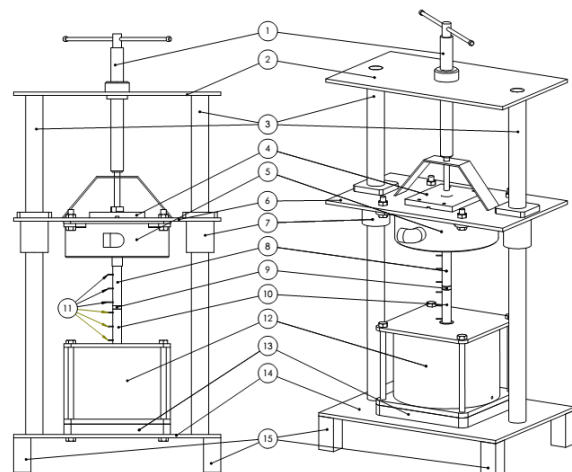


Figure 2. Thermal conductivity testing apparatus design (1) pressing handle (2) top base plate (3) vertical rod (4) load cell (5) cooling unit (6) middle base plate (7) bearing linear (8) cold meter bar (9) specimen (10) hot meter bar (11) thermocouple (12) set heater (13) isolator (14) bottom base plate (15) pods

Testing Specimen

This test equipment was dedicated to measure the thermal conductivity of thin solid material with a thickness between 0.02 to 10 mm which did not

allow the thermocouple planting. Specimens which used as validation were a material with thermal conductivity of $15 \text{ Wm}^{-1}\text{K}^{-1}$ - $50 \text{ Wm}^{-1}\text{K}^{-1}$ of the medium range thermal conductivity and diameter was equal to 13mm of bar meter.

Table 1 The applied material for validation

Material	$k \text{ (Wm}^{-1}\text{K}^{-1})$ ($50^\circ\text{C} - 400^\circ\text{C}$)
Stainless steel	~15 – 20 [9]
Bronze	~50 – 59 [1, 10]

RESULT AND DISCUSSION

Thermal conductivity testing apparatus with the ability to evaluate the solid material at a high temperature to 400°C has been created. Its design was the novelty of standard ASTM D 5470-06 which using axial heat flow approach at steady state. It has been validated by tests were performed using several materials and the results compared with the results of the thermal conductivity test Transient Hot Bridge (THB 500) of LINSEIS, the results were as follows.

Initial Validation

Thermoelectric materials have a medium thermal conductivity or thermal conductivity value be minimized [5]. It was applied to evaluate thermoelectric material with medium ranged thermal conductivity, so it was necessary to be validated using reference material of medium thermal conductivity. The material to be used as a validation were stainless steel and bronze since it has $15 \text{ Wm}^{-1}\text{K}^{-1}$ to $40 \text{ Wm}^{-1}\text{K}^{-1}$ of conductivity.

This material was previously tested using a thermal conductivity test THB 500 LINSEIS at room temperature. While, the initial validation was carried out at 50°C of temperature was a minimum working temperature of testing equipment. The difference of a minimum working temperature and THB apparatus temperature will be compared with some assumptions. Table 2 portrays the testing results using THB 500 LINSEIS test equipment at room temperature.

Table 2. Conductivity thermal test result using THB 500 LINSEIS testing apparatus

Attempt	Stainless steel		Bronze	
	$k \text{ (Wm}^{-1}\text{K}^{-1})$	T ($^\circ\text{C}$)	$k \text{ (Wm}^{-1}\text{K}^{-1})$	T ($^\circ\text{C}$)
1	14.9158	31.22	38.8946	29.50
2	14.9237	31.16	38.1200	29.40
3	14.9838	31.10	38.1503	29.30
4	14.7789	31.07	36.4067	29.40
5	14.8028	31.06	38.4993	29.50
Mean	14.8810	31.12	38.0142	29.42

• Stainless Steel Test

The first material that used as a validation was stainless steel. The test results of THB 500 LINSEIS instrument, stainless steel thermal conductivity at 31.12°C of temperature was $14.88 \text{ Wm}^{-1}\text{K}^{-1}$. The test results will be compared with the thermal conductivity reference from Bogaard [9] which was

recommended by Jensen, et al. [6] and Sweet, et al. [8]. Thermal conductivity values which were most closely the test results using it was stainless steel 304 (SS304) with $14.99 \text{ Wm}^{-1}\text{K}^{-1}$ at 31.12°C of temperature difference of 0.73%. It can only validate material at room temperature, then as a comparison at 50°C of temperature which can be used for Bogaard thermal conductivity of stainless steel material 304 ie $15.28 \text{ Wm}^{-1}\text{K}^{-1}$ @ 50°C .

Table 3 Stainless steel conductivity test result at 50°C

Attempt	k_{uji} ($\text{Wm}^{-1}\text{K}^{-1}$)	k_{ref} ($\text{Wm}^{-1}\text{K}^{-1}$)	Selisih (%)
1	15,55	15.28	-1.73%
2	15,64	15.28	-2.35%
3	16,24	15.28	-6.25%
4	15,55	15.28	-1.74%
5	15,39	15.28	-0.69%
Mean	15,67	15.28	-2.55%
Deviation standard	0,33		

Table 3 displays test data SS304 thermal conductivity, the best data was obtained on 5th attempt with a margin of literature by -0.69%, and the biggest difference was -6.25% on the 3rd. It demonstrates a good test apparatus which has an ability to validate a stainless steel with an average literature difference only by -2.55% to a standard deviation of 5th tests was $0.33 \text{ Wm}^{-1}\text{K}^{-1}$ or 2.09%.

• Commercial Bronze Test

Commercial bronze was only analyzed at a 29.42°C of temperature with a thermal conductivity value of $38.01 \text{ Wm}^{-1}\text{K}^{-1}$, it was not found in the high temperature literature. The bronze thermal conductivity can be compared at room temperature only. While, bronze properties can observed on literature at 27°C to 127°C of temperature which was fixed value, and at a temperature of 127°C to 227°C it was growing [1, 10]. Thus, the testing results at 50°C temperature was assumed to be validated with the testing results which using THB 500 LINSEIS test equipment at 29.42°C of temperature. From Table 4.3 shows the results of five times the thermal conductivity testing of commercial bronze at 50°C , with the best test results in 4th attempt by a margin of 1.21% and the biggest difference in 1st trial by a margin of 5.38%. standard deviation of 5th experiment was $1.20 \text{ Wm}^{-1}\text{K}^{-1}$ or 3.23%.

Table 4 A bold commercial bronze conductivity test result at 50°C

Attempt	k_{uji} ($\text{Wm}^{-1}\text{K}^{-1}$)	k_{ref} ($\text{Wm}^{-1}\text{K}^{-1}$)	Selisih (%)
1	35,97	38,01	5,38%
2	38,94	38,01	-2,43%
3	36,34	38,01	4,40%
4	37,55	38,01	1,21%
5	36,54	38,01	3,88%
Mean	37,07	38,01	2,49%
Deviation standard	1,20		

• Initial Validation Conclusion

In the initial validation, good results was shown from testing for each test sample with material test

ability of medium thermal conductivity ($15 \text{ Wm}^{-1}\text{K}^{-1}$ to $40 \text{ Wm}^{-1}\text{K}^{-1}$) at 50°C . The test results was indicated from two materials testing with the difference of THB 500 LINSEIS test apparatus less than 3%, this suggests a fairly accurate test equipment. Other than that, of the five-time testing this tool also showed good repeatability with a standard deviation of less than 3.5%, this indicates that the test tool has made sufficient precision.

Uncertainty Analysis

Uncertainty analysis was performed to estimate how the uncertainty in any measurement of thermal conductivity test apparatus created. It was determined using the Kline and McClintock [11] method which was formulated as following equation:

$$w_k = \left[\left(\frac{\partial k}{\partial q_{ave}} w_{q_{ave}} \right)^2 + \left(\frac{\partial k}{\partial t} w_t \right)^2 + \left(\frac{\partial k}{\partial A_1} w_{A_1} \right)^2 + \left(\frac{\partial k}{\partial \Delta T} w_{\Delta T} \right)^2 \right]^{1/2}$$

The uncertainty calculation result for each specimen as follows:

Test materials	Thermal conductivity ($\text{Wm}^{-1}\text{K}^{-1}$)
Stainless steel 304	$15,67 \pm 1,61$
Commercial Bronze	$37,07 \pm 2,13$

High Temperature Validation

The thermal conductivity high temperatures

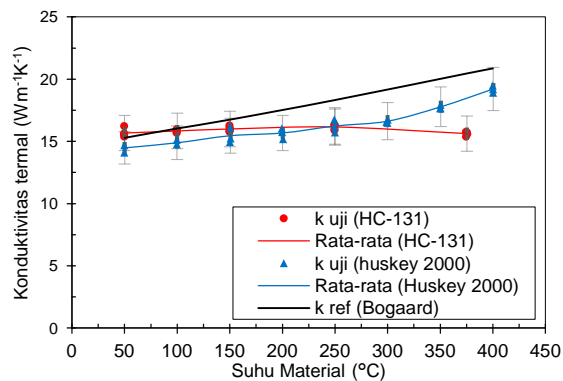


Figure 3 Stainless steel thermal conductivity test result at 50°C to 400°C

result were presented in Figure 3, where testing was done at 50°C to 400°C of temperature at rising intervals of 50°C and were included per cent uncertainty at each test with a value of $\pm 9\%$. SS304 reference for high temperature were also obtained from Bogaard, et al. [12], which demonstrating the thermal conductivity value of SS304 which rised with expanding temperatures.

One thing that will greatly affect the resulting error of the comparative method was their thermal contact resistance [13]. Test equipment which created has a testing thin material specification, and did not allow the thermocouple planting on sample materials. Therefore, to determine the material surface temperature (TH and TC) can only be done by calculation. Therefore, thermal contact resistance will greatly affect the test results. Meanwhile, testing which conducted by Jensen, et al. [6] by the same method, allowing the thermocouple planting to the

elongated material specimens. Thus, their thermal contact resistance did not significantly affect the thermal conductivity calculation for TH and TC were directly measured using a thermocouple (comparison testing scheme is shown in Figure 4. By these testing times, there were between the two meter bars materials were neglected, it needs various ways to minimizing the thermal contact resistance. Firstly, it will decrease if the connection between the pressure increased, however too much pressure can damage

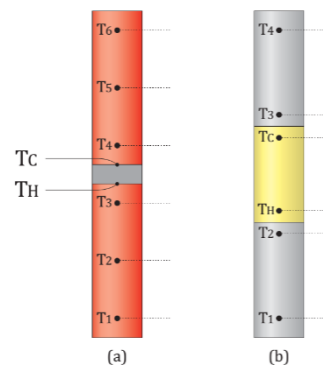


Figure 4. An axial heat flow testing method scheme thermocouple planting variations on material; (a) material planting of created test apparatus, (b) material placement dan thermocouple planting on Jensen study.

the specimen and cause deformation of the contact surfaces [14, 15]. According to ASTM D5470-06 [14] the pressure testing can be classified to some hardness materials. For soft materials, it can be used 0.069 MPa (10 psi) while the hard material of 3.4 MPa (500 psi) of pressure. The material which was engaged as validation was metallic bronze and stainless steel that can be classified as a hard material, thus pressure on the test of 3.4 MPa or 46.0 kg with the cross-sectional area of $1.33 \times 10^{-4} \text{ m}^2$. Secondly, thermal contact which can be minimized by applying a thermally conducting liquid or it-called thermal grease such as silicone oil to its surface before pressed. When the surfaces which tangent was pressed, there will always be air cavities on its surface although with a very smooth surface. The cavities were filled with air, a very low thermal conductivity ($0,024 \text{ Wm}^{-1}\text{K}^{-1}$) which resulting in a high resistance. The theory of thermal grease is to replace the low thermal conductivity of air using liquid material with higher thermal conductivity [1, 15]. There were two materials that will be used as a thermal grease on testing this time, the HC-131 was used as the initial validation at 50°C which was produced by ShenZhen Bonyx Electronics Co., LTD and Huskey 2000 Lubricant paste and Anti-Seize for High Temperature was produced by Husk-ITT Corporation.

In figure 3 are shown the testing results of both thermal grease at the same pressure. The test results show if using the thermal grease HC-131, at a temperature of 50°C to 200°C , the difference with

literature was lower by -2.55%. But the difference was getting up when the temperature rised from 250°C to 375°C with a maximum difference of 23.6%. Meanwhile, if using Huskey, 2000, at a low temperature difference from the literature of 5.27%, which higher than using HC-131. However, at high temperature difference was relatively constant temperature of 250°C to 400°C of 7.93%. The results were likely to go down at high temperatures when using HC-131 due to its thermal grease properties, that was only operating capability at a temperature of -30°C to 150°C. Therefore, at above 200°C of temperature the differences with literature were the greater because its thermal grease dried. After that, the dried thermal grease causes air to fill a contact pores between the sample to the meter bar. In addition to obstruct heat transfer due to its low thermal conductivity, the air also causes corrosion of the copper which used as meter bar material. Temperatures increased corrosion on copper rapidly, Therefore, the copper surface was formed of two layers covering the copper. The corrosion inner layer was Cu₂O and the outer layer consists of CuO and Cu₂O [16, 17]. This layer raised the contact resistance between the meter bar with a bigger sample, as a result the thermal conductivity test products utilizing HC-131 decreased when the temperature further rised.

Different things demonstrated by a test which employing Huskey 2000 as thermal grease. The test results were more stable when the testing at low or high temperatures, due to the ability of Huskey 2000 was capable of operating up to a temperature of 1093.33°C (2000 ° F). In addition, the maximum temperature that can be achieved was higher at 400°C with the same heater power 858 Watt, which exhibiting better thermal conductivity at high temperatures. Therefore, the maximum temperature can be achieved was higher also. The testing results

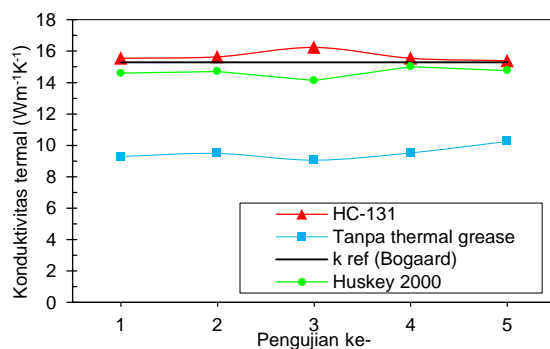


Figure 5 Thermal conductivity testing comparison of stainless steel which utilizing thermal grease HC-131, Huskey 2000 and without thermal grease at 50°C

at 50°C to 200°C produces below the HC-131, due to the conductivity of the HC-131 thermal 4 larger (0.62 Wm⁻¹K⁻¹) compared to Huskey 2000 with its main function as a lubricating oil and anti-seize. However, the Huskey 2000 applications showed the better

results compared with air or without using the thermal grease, this case is shown in Figure 5 the comparative testing product of the thermal grease utilization HC-131, Huskey 2000, and without the thermal grease. The test exhibits if no thermal grease was very much difference from the literature of 37.72%.

CONCLUSION

From these results, it can be concluded that:

1. Thermal conductivity test apparatus with axial heat flow method approach to heat flow in steady state was created by the standard ASTM D 5470-06. Where this test allows testing of thin materials without planting a thermocouple in the test sample. Using two meter bars, above, and below material to determine heat transfer rate and surface temperature of the test sample. High temperature testing that can be achieved is 400°C
2. The ability of thermal conductivity testing apparatus of the material at a temperature range of 50°C to 400°C was good enough. By the material initial validation which used stainless steel and bronze by a margin of literature by 2.55% and 2.44% and the standard deviation of the five tests of 2.09% and 3.23% which demonstrated accuracy and precision tools were pretty good. For validation, at high temperatures was showed good results also by a margin of 7.93% of the literature on the highest temperature of 400°C.

ACKNOWLEDGEMENT

This research was supported by Grants Research PUPT (Commodity Research Universities) Sebelas Maret University, Surakarta.

REFERENCE

- [1] Y. A. Cengel, *Heat & Mass Transfer: A Practical Approach*: McGraw-Hill Education (India) Pvt Limited, 2007.
- [2] J. P. Holman, *Heat Transfer* vol. Tenth Edition. New York: McGraw-Hill, 2010.
- [3] S. Reif-Acherman, "Early and current experimental methods for determining thermal conductivities of metals," *Elsevier*, vol. 77, pp. 542–563, 20 May 2014 2014.
- [4] A. Kurniawan, "Pengembangan Semikonduktor Tipe-P untuk Modul Termoelektrik Berbasis Material ZnO," Universitas Sebelas Maret Surakarta, 2014.
- [5] H. J. Goldsmid, *Introduction to Thermoelectricity*: Springer Berlin Heidelberg, 2012.
- [6] C. Jensen, C. Xing, C. Folsom, H. Ban, and J. Phillips, "Design and Validation of a High-Temperature Comparative Thermal-Conductivity Measurement System," *International Journal of Thermophysics*, vol. 33, pp. 311-329, 2012.

- [7] T. Dasgupta and A. Umarji, "Apparatus to measure high-temperature thermal conductivity and thermoelectric power of small specimens," *Review of scientific instruments*, vol. 76, p. 094901, 2005.
- [8] J. N. Sweet, E. P. Roth, and M. Moss, "Thermal conductivity of Inconel 718 and 304 stainless steel," *International Journal of Thermophysics*, vol. 8, pp. 593-606, 1987.
- [9] R. H. Bogaard, "Thermal Conductivity of Selected Stainless Steels," in *Thermal Conductivity 18*, T. Ashworth and D. R. Smith, Eds., ed Boston, MA: Springer US, 1985, pp. 175-185.
- [10] F. P. Incropera, T. L. Bergman, and A. S. Lavine, *Fundamentals of Heat and Mass Transfer*: Wiley, 2011.
- [11] S. J. Kline and F. McClintock, "Describing uncertainties in single-sample experiments," *Mechanical engineering*, vol. 75, pp. 3-8, 1953.
- [12] R. H. Bogaard, P. D. Desai, H. H. Li, and C. Y. Ho, "Thermophysical properties of stainless steels," *Thermochimica Acta*, vol. 218, pp. 373-393, 1993/05/03 1993.
- [13] T. M. Tritt, *Thermal Conductivity : Theory, Properties, and Applications*. 233 Spring Street, New York: Kluwer Academic / Plenum Publishers, 2004.
- [14] ASTM D5470-06, "Standard Test Method for Thermal Transmission Properties of Thermally Conductive Electrical Insulation Materials " in *ASTM Standard* vol. D 5470-06, ed. West Conshohocken, United States: ASTM International, 2006.
- [15] J. P. Holman, *Experimental methods for engineers* vol. 8th edition. 1221 Avenue of the Americas, New York, NY 10020: The McGraw-Hill Companies, Inc, 2012.
- [16] C. D. S. Tuck, C. A. Powell, and J. Nuttall, "Corrosion of Copper and Its Alloys," in *Reference Module in Materials Science and Materials Engineering*, ed: Elsevier, 2016.
- [17] Y. Wan, X. Wang, H. Sun, Y. Li, K. Zhang, and Y. Wu, "Corrosion Behavior of Copper at Elevated Temperature," *International Journal of Electrochemical Science*, vol. 7, p. 7902, 2012.

THE UTILIZING CUTTING FLUID AND FEEDING RATE EFFECT TO THE SURFACE HARDNESS AND PRECISSION OF ALUMINUM MATERIAL USING CNC MILLING MACHINE

Widhaya Bastian Purnama¹, Indri Yaningsih², Heru Sukanto²

¹Program Sarjana Jurusan Teknik Mesin – Universitas Sebelas Maret

²Staf Pengajar – Jurusan Teknik Mesin – Universitas Sebelas Maret

Keywords :

Cutting Fluid
Feed Rate
Surface Roughness
Precision

Abstract :

There are many factor affecting the quality of product that are produced from milling machine process. The quality is mostly about surface roughness and precision. Those affecting factors are the selection of cutting parameter and use of cutting fluid. The research is done in order to know the effect of using cutting fluid and feed rate to aluminum on surface roughness and precision using Milling CNC machine. This research uses milling CNC Mitsubishi M70 machine. The free variables of feed rate are 20, 32, 45, 69, 108 mm/min. Each feed rate variations are given cutting fluid and no- cutting fluid treatment. The cutting fluid used is bromus oil which is mixed with water. The tests performed were surface roughness test, precision test. The result of this study shows that feed rate is in line with surface roughness. The use of cutting fluid affects surface roughness. The surface roughness score at feed rate variation using coolant treatment are 20, 32, 45, 69, 108 mm/min shows the surface roughness score of 0,442; 0,484; 0,553; 0,643; 0,797 μm . surface roughness score without cutting fluid treatment reveals the score of 0,470; 0,517; 0,582; 0,662; 0,847 μm . According to statistical analysis result using two way ANOVA, it can be concluded that the use of cutting fluid and feed rate affect precision at 95% trust rate. The measurement of A dimension using cutting fluid in the variation of feed rate 20, 32, 45, 69, 108 mm/min shows the precision rate of 99,999348; 99,99929; 99,999304; 99,999261; 99,9992 %. While, the variation without cutting fluid treatment reveals the precision rate at 99,999188 ; 99,999184; 99,999037; 99;998884; 99,998684 %.

PENDAHULUAN

The development of science and technology nowadays, especially manufacturing industry is required to improve product quality, production speed, and production costs in order to compete with others. It requires a solution to solve the problem. One of them with a CNC machine. CNC machine is a machine which controlled by a computer using numerical language (command data with the code numbers, letters, and symbols) according to ISO standards. CNC technology working systems will be more synchronized between computers and mechanics. Therefore, when it compared with similar machine tools, CNC machine tools, more accurate, more precise, more flexible, and suitable for mass production. A designed CNC machine is to support the production of which requires a high level of complexity.

The ideal geometry characteristics of a product or a component of which is precision and smooth surface. A surface smoothness and precision are an important role in component planning which related to the friction lubrication problems, worn-out, and

fatigue resistance. In [1] study exhibited that the feed rate is the most influential parameter toward the end of the surface roughness on the aluminum samples. Besides the feed rate, cutting fluid applications also assessed affect the surface roughness.

From the above background, it is necessary to expand research on the effects of cutting fluid application and feed rate selection to the surface roughness and the accuracy level. This study is expected to recognize the manufacturing process utilizations and election.

LITERATURE REVIEW

[2] conducted a study on the cutting fluid operation in machining process. Various methods have been used to protect the chisel from the heat which generated during the machining process. The coated cutting tool selection is an expensively alternative and generally suitable for some materials such as titanium alloys, heat-resistant alloys, etc. Another alternative is to implement the cutting fluid utilization in engine operation. Cutting fluid is used for lubricating and fluid cutting effect between

cutting tool and workpiece, chisel and chips during the engine is operated. Therefore, the heat generated effect on the cutting tool can be prevented. The research produced the cutting fluid selection for the machining process which generally provides benefits such as extending its service life and chisel, improve the surface finishing quality and dimensional accuracy better.

[3] performed a research on the spindle speed effect, feed rate, and the chisel slope using an end mill chisel to surface roughness. It was using a milling machine, the independent variable was 700, 800, 900 rpm of spindle speed, 100, 200, 300 mm/min of feed rate, and 10, 30, 50 of tilt angle. It was employing a ball nose end mill chisel of diameter 10 mm. These studies were concluded that the larger feed rate, the greater surface roughness (proportional). While the greater spindle speed and slope, the smaller surface roughness was obtained (inversely). The lowest surface roughness parameters was obtained at 9 rpm of spindle speed, 100 mm/min of feed rate, and the slope of cutting tool was 50 with 0.58667 harshest lm.

Cutting Fluid

Cutting fluid was exploited in metal cutting or machining process for several reasons, for instance, to extend tool life, reduce the workpiece deformation due to heat, improve the surface quality machining results, and clean growled from cut surfaces. It was utilized that can be categorized into four types::

- Straight oils
- Soluble oils
- Synthetic fluids
- Semisynthetic fluids

Surface Roughness Parameters

To producing a surface profile, sensor/ feeler (stylus) measurement tool must be moved to follow the trajectory was a straight line with a predetermined distance in advance. The path length was referred to the transversing length. Shortly after needle was moving and it stopped shortly before the electronic measuring instruments perform calculations based on the data detected by needle probe. Length measurements section where the surface profile analysis referred to the sample length. Actual reproduction profile is as shown in Figure 1:

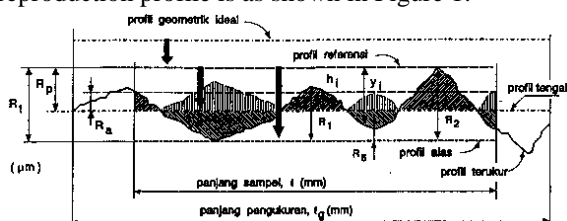


Figure 1. A surface profile [4]

Based on the profiles described above, it can be defined that several parameters of the surface, which are related to the dimensions in the direction vertical

and horizontal direction. Vertical dimension is known for some parameters, namely:

Total roughness, R_t (μm).

Is the distance between the reference profile with a profile board.

Arithmetic average roughness, R_a (μm).

Is an arithmetic average value from absolute value of the distance between the profiles that measured by the middle profile.

$$R_a = \sqrt{\frac{1}{l} \int_0^l h_i^2 dx}$$

Total roughness mean, R_z (μm).

Is the pedestal profiles average distance to measured profiles on the five highest peaks, which reduced by pedestal profile average distance to measured profiles on five lowest valleys.

$$R_z = \frac{\sum[R_1 + R_2 + \dots + R_5 - R_6 - \dots - R_{10}]}{5}$$

Precision

Precision shows value how close the difference at the time of measurement repeatability. Although, the measurement accuracy results indicates closeness to the true value. The definition can be described in the following illustration.

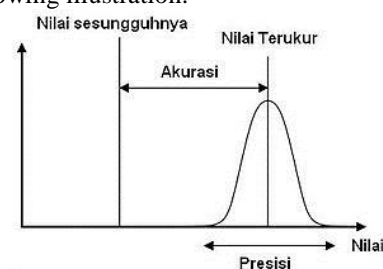


Figure 2. Precision and Accuracy Illustration

In the field of science, industrial engineering, and statistics, the accuracy measurement system is a measurement of the closeness level to the true value. Precision measurement system, also called reproducibility or repeatability is the extent to which measurement repeated in an unchanging state get the same results. A measurement can be accurate and precise, or accurate but not precise or accurate but not precise, or the inaccurate and imprecise [5].

RESEARCH METHODOLOGY

This research was conducted at Laboratory of National Electric Car, Mechanical Engineering, Universitas Sebelas Maret, Surakarta.

The material which used in this study was Aluminium. Chisel was used with carbide cutting tool material with a chisel type and diameter as follows:

- Endmill carbide 20 mm (facing).
- Endmill carbide 10 mm (profil).
- Drill chisel diameter 5 mm.
- Chisel thread M06x1.

The material which employed in this study was Aluminium. Chisel material was carbide cutting tool with a chisel type and diameter as follows:

5. Endmill carbide 20 mm (facing).
6. Endmill carbide 10 mm (profil).
7. Drill chisel diameter 5 mm.
8. Chisel thread M06x1.

Independent Variable

The independent variable is a variable which determined by investigators and the value can be changed by a certain method to get the dependent variabel amount of the research object, to obtain correlation between them. In this research, there two independent variables were cutting fluid (with and without) and feed rate (20, 32, 45, 69, 108 mm/ min).

Dependent Variable

The dependent variable is a variable whose value depends on the independent variables and identified after an investigation. The corelation between independent and dependent variables will produce changes of dependent variable value. The dependent variable in this study was the result of surface roughness and precision machining processes

Controlled Variable

Controlled variable is a variable whose value is kept constant during the study. It were kept constant during this study include 800 rpm of spindle rotation (facing) and 1600 rpm (profil), and 1 mm of feeding depth.

The initial stage of this study was began by creating 3D modeling using solidworks software. The design was made that the motor vehicle spare parts named Engine Kill Switch. Work piece design is shown in Figure 3.

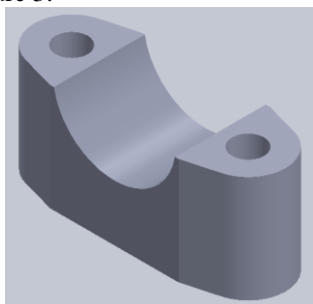


Figure 3. Work piece cross section design.

Experiments simulation was using solidcam software, and from the simulation results will be obtained which employing the NC-Code with post processor that suitable with CNC machines was used, MITSUBISHI M-70.

An initial machining process by employing a CNC milling machine which was facing process that using independent variables that have been determined. After it completed, followed by surface roughness measurements, using Surface Roughness

Tester SJ-201 series. At the time of data capture, sensors position constantly moved which suitable with horizontal axis and parallel to the test object (that were in a straight line).

The next machining process was profile manufacturing process with the same independent variables treatment. Afterthat, data collection was performed to determine the dimensions of precision. Each workpiece measurement was done in four different positions as shown in Figure 4.

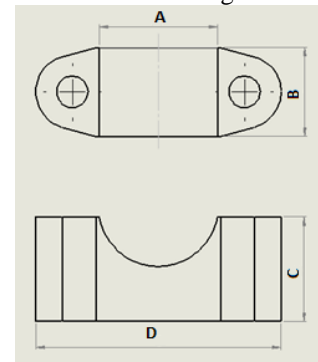


Figure 4. Workpiece measurement dimensions area

RESULT AND DISCUSSION

The surface roughness testing results of cutting fluids application and selection of feed rate can be seen in Figure 5.

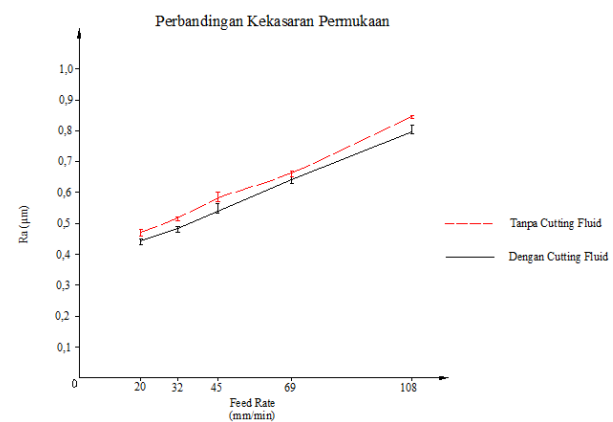


Figure 5. Diagram of feed rate variations with and without cutting fluid to surface roughness correlation

Figure 5 portrays in feed rate variations with and without cutting fluid to the surface roughness correlation of the workpiece. The testing result which was using cooler showed graphs that the surface roughness of each variation of the feed rate was raised. Roughness values on variations of 20, 32, 45, 69, 108 mm/ min of feeding rate which empolyng a cutting fluid, it was demonstrating by 0.442; 0.484; 0.553; 0.643; 0.797 lm respectively. On the other treatments, ie without a cutting fluid testing the surface roughness as shown in Figure 3. It displays an the surface roughness of each variation of the feed rate of the feed rate low to high feed rate was

increased. The surface roughness variations of 20, 32, 45, 69, 108 mm/ min of feeding rate without using a cutting fluid exhibits 0,470; 0,517; 0,582; 0; 662; 0,847 lm of roughness. From Figure 5 above demonstrates that feeding rate was directly proportional to the surface roughness. The greater feeding rate, the larger surface roughness was obtained which was practicing with or without it. This was convenient to [6] research which was stated that the higher feeding rate, the huge machining process surface roughness of CNC milling, as the same as low feed rate, the surface roughness will be smaller.

The cutting fluid application on a CNC milling process was performed on the aluminum material which effected on the surface roughness. This is shown in the graph in which the roughness value variation of 20, 32, 45, 69, 108 mm/ min of feeding rate that using a cutting fluid, establishing the roughness value by 0.442; 0.484; 0.553; 0.643; 0.797 lm respectively. The surface roughness values without using cutting fluid demonstrated 0,470; 0,517; 0,582; 0; 662; 0,847 lm of roughness. Workpiece which was using cutting fluid treatment has a less roughness than without treatment. One of the cutting fluid functions was to reduce built-up edge. It is one of the major contributing factors in the natural surface roughness. It can be continuously formed and broken, the fault will be borne particles below the surface of the chip and the new workpiece surface. Therefore, chip that was formed will be larger, it will produce a rougher surface. By reducing built up edge, then the resulting surface will be finer [7]. The basis of the theory stated that the cutting fluid utilization have an effect on the workpiece. Ie, the workpiece surface was produced become finer [8]. This was suitable to research which conducted by [1] which tells that cutting fluid application will affect the final surface output. There was also a study of [3] which declares that the greater feeding rate, the greater surface roughness (proportional).

Dimensional measurements was engaging calipers measuring devices with an accuracy of 0.01 mm. Dimensional measurements was carried out 30 times against 10 different workpieces, each workpiece 4 times measurements at different positions. The data obtained in this test data was contained data dimensions of the measurement position A, B, C, D.

The measurement results were then analyzed using Variance two-way (two way ANOVA) analysis to investigate whether there was any difference some treatments effects (the cutting fluid utilization and feeding rate) on the dependent variable (data precision) using SPSS (Statistical Product and Service Solution) version 22 ,

On entering the data in the table to be analyzed, the researchers exploited the distance between dimensions measured data with an overall average of each sample. The distance between the average

measured dimensions can be defined as following formula:

$$d_n = -(x_n - \bar{x})^2$$

Where:

d_n : Input data (average measured dimensions)

x_n : Spot sample each measurement

\bar{x} : Average measurement each sample

Based on SPSS program calculations was obtained the following results :

Table 1. Program SPSS Dimension A Results Analysis

Tests of Between-Subjects Effects

Dependent Variable: dimensiA

Source	Type III Sum of Squares	Df	Mean Square	F	Sig.
Corrected Model	3,58E-5 ^a	9	3,98E-6	6,399	,000
Intercept	9,61E-5	1	9,61E-5	154,418	,000
feedrate	1,28E-5	4	3,21E-6	5,165	,000
cuttingfluid	1,38E-5	1	1,38E-5	22,195	,000
feedrate * cuttingfluid	9,17E-6	4	2,29E-6	3,685	,006
Error	,000	290	6,22E-7		
Total	,000	300			
Corrected Total	,000	299			

a. R Squared = ,166 (Adjusted R Squared = ,140)

Table 2. Program SPSS Dimension B Results Analysis

Tests of Between-Subjects Effects

Dependent Variable: dimensiB

Source	Type III Sum of Squares	df	Mean Square	F	Sig.
Corrected Model	5,32E-6 ^a	9	5,91E-7	16,248	,000
Intercept	9,91E-6	1	9,91E-6	272,401	,000
feedrate	2,26E-6	4	5,66E-7	15,571	,000
cuttingfluid	2,10E-6	1	2,10E-6	57,957	,000
feedrate * cuttingfluid	9,45E-7	4	2,36E-7	6,498	,000
Error	1,05E-5	290	3,63E-8		
Total	2,57E-5	300			
Corrected Total	1,58E-5	299			

a. R Squared = ,335 (Adjusted R Squared = ,315)

Table 3. Program SPSS Dimension C Results Analysis

Tests of Between-Subjects Effects

Dependent Variable: dimensiC

Source	Type III Sum of Squares	df	Mean Square	F	Sig.
Corrected Model	2,32E-5 ^a	9	2,58E-6	9,227	,000
Intercept	3,81E-5	1	3,81E-5	136,275	,000
feedrate	5,63E-6	4	1,40E-6	5,032	,001
cuttingfluid	1,45E-5	1	1,45E-5	52,049	,000
feedrate * cuttingfluid	3,04E-6	4	7,60E-7	2,717	,030
Error	8,11E-5	290	2,79E-7		
Total	,000	300			
Corrected Total	,000	299			

a. R Squared = ,223 (Adjusted R Squared = ,198)

Table 4. Program SPSS Dimension D Results Analysis

Tests of Between-Subjects Effects

Dependent Variable: dimensiD

Source	Type III Sum of Squares	df	Mean Square	F	Sig.
Corrected Model	2,562E-5 ^a	9	2,846E-6	9,663	,000
Intercept	4,219E-5	1	4,219E-5	143,256	,000
feedrate	7,850E-6	4	1,963E-6	6,663	,000
cuttingfluid	1,405E-5	1	1,405E-5	47,697	,000
feedrate * cuttingfluid	3,717E-6	4	9,292E-7	3,155	,015
Error	8,542E-5	290	2,945E-7		
Total	,000	300			
Corrected Total	,000	299			

a. R Squared = ,231 (Adjusted R Squared = ,207)

Based on SPSS analysis table result shows that the significance level of feeding rate correlation to accuracy was <0.05 (significance level has been determined) so H_{0A} was rejected. Therefore, the H_{1A} decision test, which means there was influence between feeding rate to precision. Significance value of the precision correlation to cutting fluid was <0,05 so H_{0B} was also rejected. It can be concluded that there was influence between the cutting fluid applications to precision. Similarly, the significance value level of feeding rate correlation and cutting fluid <0.05. Thus, H_{0AB} was rejected and accepted H_{1AB} which means there was an interaction between feed rate and cutting fluid toward precision.

To find the deployment of data, researchers determined the standard deviation in each dimension in a variety of independent variables. The smaller standard deviation, the deployment of data was taken increasingly accumulate. Futhermore, standard deviation can be determined using the formula:

$$S = \left[\frac{\sum_{i=1}^{i=n} (x_n - \bar{x})^2}{n - 1} \right]^{1/2}$$

Once distributing data was known on each sample, and then look for accuracy value using the formula:

$$\text{Precision} = \left(100 \% - \sum_{i=1}^{i=n} \left| \frac{x_n - \bar{x}}{\bar{x}} \times 100 \% \right| \right)$$

The graph of feeding rate to cutting fluid application variations to the accuracy level of observation results are shown in the following figures:

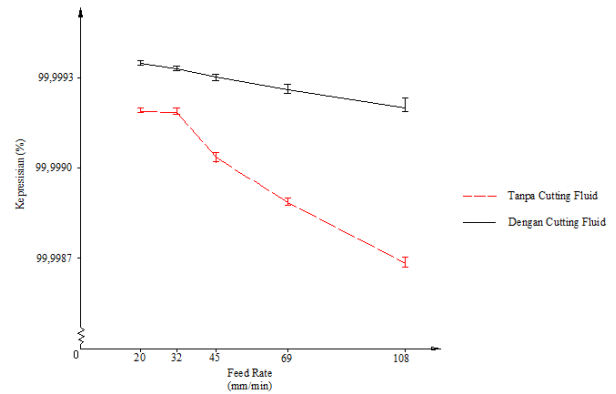


Figure 6. Feeding Rate to Precision Correlation Graph of a Half Circle Observation Results Data (A)

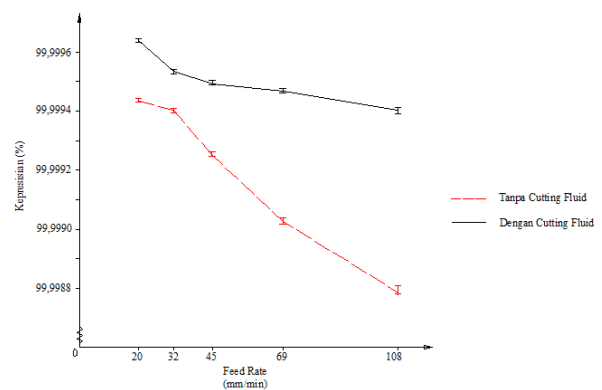


Figure 7. Feeding Rate to Precision Correlation Graph of Width Dimensions Observation Results Data (B)

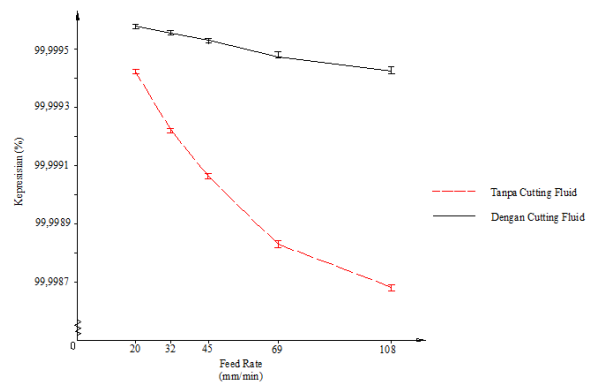


Figure 8. Feeding Rate to Precision Correlation Graph of Height Dimensions Observation Results Data (C)

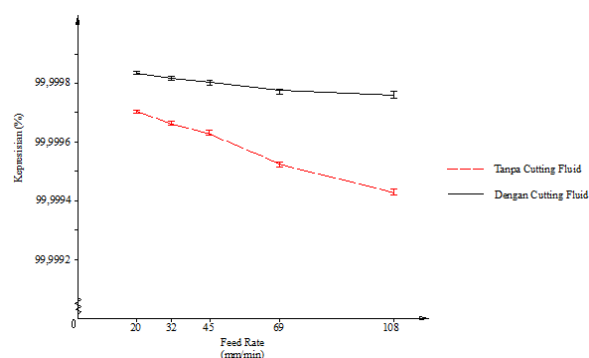


Figure 9. Feeding Rate to Precision Correlation Graph of Length Dimensions Observation Results Data (D)

From the graphs above show the cutting fluid effect and feeding rate variations on precision. The higher feeding rate, the lower the precision level. It may be caused of the vibration which generated by the friction between cutting tool to the workpiece. The greater feeding rate, the huge vibration was obtained [6]. If the vibrations was produced high, the workpiece precision will be decreased. The cutting fluid applications variations, indicating that it showed a higher level of accuracy than without employing it. One of the cutting fluid utilization was to reduce built-up edge. Built up edge is one of the major contributing factors in the natural surface roughness and precision. Built up edge can be continuously formed and broken, the fault will be borne particles below the surface of the chip and the new workpiece surface. Therefore, chip that was formed will be larger, it will exhibit a rougher surface and precision. By reducing built up edge, then the resulting surface will be better [7]. These results were suitable with studies that conducted by [2] suggested that cutting fluid employment for the machining process generally provides benefits to improve the surface finish quality. It was also consistent with the theory that one of the cutting fluid operation benefits of which was the workpiece surface to be better [8].

CONCLUSION

Based on data analysis and discussion could be taken several conclusions as follows:

1. The higher feeding rate, the greater surface roughness. The cutting fluid application has a positive influence on the surface roughness was denoted by the roughness 20, 32, 45, 69, 108 mm/min of feeding rate of it, demonstrating the roughness value by 0.442; 0.484; 0.553; 0.643; 0.797 μm respectively compared with the same feeding rate without it displays 0,470; 0,517; 0,582; 0,662; 0,847 μm of surface roughness value.
2. The cutting fluid and feeding rate variations was known to affect the precision of the test two way ANOVA hypothesis with 95% of satisfaction level. The higher feeding rate, the accuracy level

was getting lower. The cutting fluid utilization caused a higher level of precision.

REFERENCE

- [1] M.T., Hayajneh, Montasser, S., Tahat, J., Bluhm, *Study of Effect of Machining Parameter on Surface Roughness in the End-Milling Proces*. Vol.1 Number 1 ISSN 1995-6665. 2007.
- [2] O., Cakir, A., Yardimeden, T., Ozben, E., Kilickap, *Selection of Cutting Fluids in Machining Processes*. Journal of Achievements in Materials and Manufacturing Engineering 2007.
- [3] A. A., Rizkiani, A. A., Sonief, Purnami. *Pengaruh Spindel Speed, Feed Rate, dan Kemiringan Pahat Pada Proses Pemakanan Conventional Miring Menggunakan Pahat End Mill Terhadap Kekasaran Permukaan*. Malang: Jurusan Teknik Mesin Fakultas Teknik Universitas Brawijaya. 2013.
- [4] T., Rochim, *Spesifikasi Geometris Metrologi Industri dan Kontrol Kualitas, Laboratorium Teknik Produksi dan Metrologi Industri*. Bandung: Jurusan Teknik Mesin, FTI, ITB. 2001.
- [5] B., Armunanto, *Teknik Pengukuran (Metrologi Industri)*. Surakarta: ATMI PRESS. 2001.
- [6] A. A., Syah, E., Sutikno, R. Raharjo, *Pengaruh Feed Rate dan Depth of Cuts Terhadap Surface Roughness Pada Proses Milling Dengan Bantuan 4 Axis CNC Machine*. Malang : Jurusan Teknik Mesin Fakultas Teknik Universitas Brawijaya. 2014.
- [7] S., Muktiwibowo, E., Sutikno, T., Oerbandono, *Pengaruh Depth of Cut dan Variasi Cutting Fluid Terhadap Surface Roughness Aluminium 6061 Hasil Proses Turning*. Malang : Jurusan Teknik Mesin Fakultas Teknik Universitas Brawijaya. 2011.
- [8] D., Rahdiyanta, *Cairan Pendingin Untuk Proses Pemesinan*. Yogyakarta : Universitas Negeri Yogyakarta. 2010.
- [9] G., Boothroyd, *Fundamentals of Metal Machining and Machine Tools*. Tokyo: McGraw Hill Book Co. 1985.
- [10] S., Lubis, S. A., Yanuari, *Pengaruh Parameter Pemotongan Pada Proses Side Milling dan Face Milling Terhadap Kekasaran Permukaan Logam*. Jakarta : Jurusan Teknik Mesin Universitas Tarumanagara. 2014.
- [11] L., Kirkup, B., Frenkel, *An Introduction to Uncertainty in Measurement*. NewYork: Cambridge University Press. 2006.
- [12] A., Daryus, *Proses Produksi*. Jakarta: Universitas Darma Persada. 2008.

- [13] A. N. P., Emad, K. K. P., Ali, *Computer-Based Design and Manufacturing*. Houston, TX, USA: Springer. 2007.
- [14] F., Klocke, *Manufacturing Processes I Cutting Translated by Aaron Kuchle*. Germany: Library of Congress Control Number: 2011925556. 2011.
- [15] R. A., Patil, V. D., Shinde, H. V., Shete, S. P., Nevagi, *Effect of High Pressure Coolant on Surface Finish in Turning Operation*. International Journal of Innovative Research in Science, Engineering and Technology, ISSN 2319-8753. 2013.
- [16] SolidCAM 2013 *Milling Training Course 2.5D Milling. 2013*. SolidCAM.
- [17] SolidCAM Milling User's Guide Volume 1. 2004. SolidCAM LTD.

WIND TURBINE VERTICAL AXIS H ROTOR TYPE WITH 1 kW CAPACITY AT SUWUK BEACH, KEBUMEN

Achmad Gustiantono¹, Dominicus DDPT², Syamsul Hadi²

¹Pelajar – Jurusan Teknik Mesin – Universitas Sebelas Maret

²Staf Pengajar – Jurusan Teknik Mesin – Universitas Sebelas Maret

Kata Kunci :

Potensi angin, Desain, Turbin angin, H-rotor

Tulisan ini membahas tentang analisa potensi energi angin di pantai Suwuk Kebumen dan perancangan turbin angin tipe H-Rotor yang sesuai dengan karakteristik angin di pantai tersebut. Analisa potensi energi angin menggunakan metode distribusi Weibull berdasarkan data kecepatan angin di lokasi pengukuran selama 2 tahun. Analisa distribusi Weibull menunjukkan karakteristik kecepatan angin di lokasi pengukuran yang akan dijadikan dasar dalam perancangan turbin angin H-Rotor. Perancangan turbin angin H-Rotor terdiri dari komponen-komponen seperti sudu, strut, dudukan strut, poros, tiang, dan generator. Diperoleh rancangan turbin angin H-Rotor dengan diameter x tinggi sebesar 2,7 x 2,7 meter menggunakan airfoil tipe NACA 0018 dengan kapasitas daya keluaran sebesar 1 kW..

Abstrak :

PENDAHULUAN

In recent years, the energy crisis that hit the world and particularly in Indonesia became a problem which is quite crucial. The fuel needs of human life is increasing, while supplies of oil or gas is very limited and can not be renewed cause oil reserves from year to year decrease dramatically.

It can be seen from the data above that oil production declining in Indonesia from year to year and 163.633 thousand barrel of crude oil production was down 50% from the previous year by 2012. In addition, due to the pollution, the global warming has been arising from the burning of fossil energy sources. It made us to enterprise for alternative energy sources that are clean and not limited to generating electricity.

Indonesia is a country with energy resources are very abundant, one of them are water and wind energy sources. Indonesia is an archipelago and one of the countries which located at the equator to be one factor why Indonesia has an overflow wind energy feasible. Its potential is quite adequate, due to 3.5 to 7 m/ s of the average wind speed ranges in Indonesia. The mapping of National Institute of Aeronautics and Space (LAPAN) at 120 locations shows some regions have wind speeds above 5 m/ sec, East Nusa Tenggara, West Nusa Tenggara, South Sulawesi, the southern coast of Java, respectively. The wind power applications as a source of renewable energy in Indonesia is very likely to be further developed [1].

The southern coast of Java has wind energy potential is tremendous with 3.5 to 7 m/ s of the average wind speed ranges. The suwuk beach become one of southern coast of Java is located in the southern city of Kebumen and used as tourist attractions. As a tourist attraction, the suwuk beach requires a supply of electrical energy among others for food stall lighting, drain the water, and the fulfillment of electricity at some recreation places.

The electrical energy source on this coast is originate from PLN and only available on a small scale by this time. In addition, the power outages is frequently happen which caused electricity shortages at Suwuk beach. Therefore, we need another energy source to overcome an electricity. A large number of wind energy potentials on Suwuk beach made wind turbine is the right choice to tackle the problem.

RESEARCH METHODOLOGY

The H-rotor wind turbine design begins with wind speed data processing by using Weibull distribution method. The Pandansimo Bantul beach wind speed data was used due to its complete and located in the same geographic of suwuk beach which placed the south coast of Java island. Data has been obtained by measuring wind speeds at the beach Pandansimo for two years from June 2013 to 2015. It was found that wind speed often arise (VF) 4.37 m/ s of wind speed while carrying 7.99 m/ s of maximum energy (VE). Based on its characteristics, calculation and determination of each component H-rotor wind turbine models can be done.

RESULT AND DISCUSSION

Wind Speed Data Processing

The wind speed data processing results was obtained during the two years from June 2013 to June 2015 by using the graphs and cumulative probability density of Weibull distribution [2], as shown in Figure 1 and Figure 2.

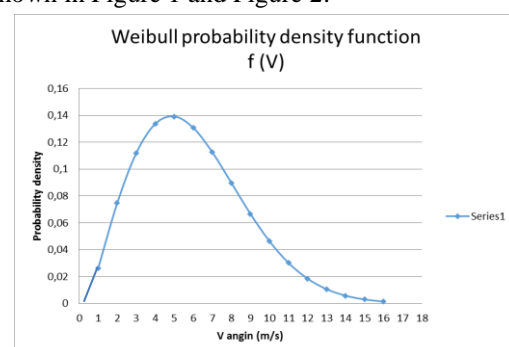


Figure 1. Density probability function

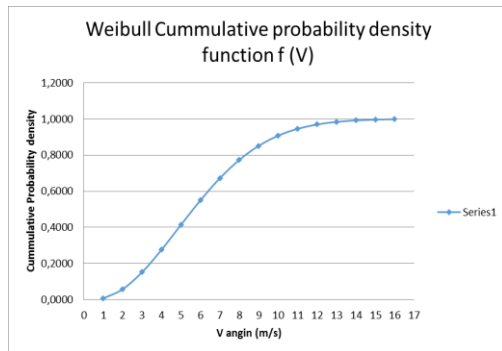


Figure 2. Cumulative Distribution Function

It can be clearly seen on Figure 1 that often frequently appears 4.37 m/ s of wind speed with 14%. Figure 2 shows the wind speed appearance chance at certain intervals. The cut-in wind speed is equal to or greater than 2 m/ s, 3 m/ s and 94.24%, 84.8% respectively.

The H-Rotor Wind Turbine Design

Hybrid turbine construction is shown in Figure 1. The components that will be constructed are blade, strut, strut mounting, shaft, mast, generator and transmission systems.



Figure 3. Vertically Axis Hybrid Wind Turbine Construction

1. Turbine Blade

Blade which was designed as a straight blade of NACA 0018 airfoil shape due to its strong and good aerodynamic construction characteristics [3]. The number of blades which used was 3 pieces that make loading variations spoon evenly by using carbon fiber material that performs corrosion resistant and strong. According to Oyedepo by 2012, wind speed design that was brought maximum energy (VE). The unknown 8 m/ s VE value, the H-rotor wind turbine size can be determined by reference [3] is

$$\begin{aligned} \text{Solidity} &= 0.24 \\ \text{Rotor diameter (D)} &= 2.7 \text{ m} \\ \text{Blade length (b)} &= 2.7 \text{ m} \\ \text{Chord length (c)} &= 0.216 \text{ m} \end{aligned}$$

$$\begin{aligned} \text{Swept area (A)} &= 7.29 \text{ m}^2 \\ \text{2. Force Analysis on Blade} \end{aligned}$$

The aerodynamics H-rotor analysis is quite complex though the rotor shape is relatively simple. As the wind strikes the blade, not only wind speed are affecting lift (L) and propulsive force (D) on the blade but also influence the relative wind speed [3].

Lift (L) is a force that perpendicular to the relative wind speed while the thrust (D) is a force that parallel to the relative wind speed. Normal force (N) is a force that is perpendicular to the chord of the blade while the axial force (A) is a force that is parallel to the chord of the blade as shown in Figure 4. The forces are calculated using the equation, [4].

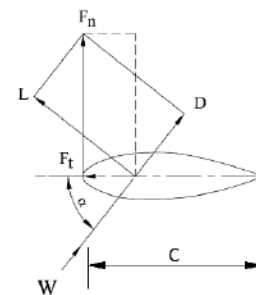


Figure 4. Turbine Blade Force Diagram

$$\begin{aligned} L &= \frac{1}{2} \rho W^2 \times Cl \times C \times H \\ D &= \frac{1}{2} \rho W^2 \times Cd \times C \times H \\ N &= L \cos \alpha + D \sin \alpha \\ A &= L \sin \alpha - D \cos \alpha \end{aligned}$$

The calculation results forces that occur on the blade indicated by Table 2. From the table it can be seen that the value of lift (L) and normal force (N) consecutive maximum of 610.36 N and 603.44 N at position angle of pitch 140°.

Table 2. Lift force, thrust, normal, and axial pitch angle variations

No	pitch angle (θ) (deg)	sudut serang (α) (deg)	Lift force (N)	Drag force (N)	Normal force (N)	Axial force (N)
1	0	0	0	0	0	0
2	30	5,75	471,23	13,53	470,21	33,72
3	60	10,66	607,67	19,83	600,86	92,89
4	90	13,71	482,47	40,48	478,33	74,97
5	120	13,54	507,45	37,06	502,04	82,7
6	140	10,93	610,36	21,83	603,44	94,25
7	150	8,81	574,71	17,29	570,58	70,9
8	180	0	0	0	0	0
9	210	-8,77	-359,04	10,83	-356,5	44
10	240	-13,52	-235,24	17,42	-163,34	13,38
11	270	-13,72	-219,87	18,74	-218,04	33,92
12	300	-10,69	-340,44	11,13	-336,6	52,18
13	330	-5,78	-348,65	10,01	-347,89	25,15
14	360	0	0	0	0	0

3. Shaft

Material for the shaft was selected AISI 4130 steel with 359 Mpa of material maximum tensile

stress. A safety factor value equal to 8 was used for steel materials [5].

Shaft diameter calculation of hybrid vertical axis wind turbine considers the style of the axis of the twisting moment (Te) and bending moment (Me), the shaft diameter (d) was obtained 90 mm.

4. Cradle Strut and Strut

a. Cradle Strut

A holder AISI 6061 of aluminum strut material was practiced with 55.15 MPa of yield strength [5]. Diameter mounting strut (D) is set at 250 mm. Stand strut under pressure due to heavy pressure turbine blade bending and compressive stress due to centrifugal force [6].

Width (b) strut is 60 mm, since there will be screw mounted to a strut, then the size of the thickness (h) strut to:

Bending compressive stress due to the weight of the turbine blade

$$a. \quad = \sqrt{\frac{2 b \sigma_d}{18 M}}$$

$$= 54,55 \text{ mm}$$

b. Press tension due to sentrifugal force

$$h = \frac{mb \times \omega^2 \times R}{b \times \sigma} \times \frac{1}{N}$$

$$= 39,05 \text{ mm}$$

then it was selected thick strut holder (h) of 39.05 mm.

b. Strut

The strut material was the same as the material for the holder strut. Strut was tensioned a bending pressure due to turbine heavy blade and compressive stress due to centrifugal force [6]. Number strut for each blade was 2 [7].

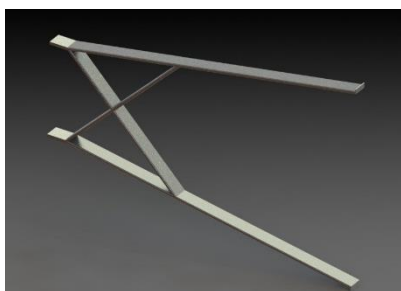


Figure 5. Strut

Width (b) strut 60 mm was taken, since there will be screw mounted to a strut, then the thickness size (h) strut against bending compressive stress due to the weight of the turbine blade

$$h = \sqrt{\frac{2 b \sigma_d}{6 M}}$$

$$= 12 \text{ mm}$$

Checking the strut dimensions has been secured against centrifugal loads then it can be calculated by the equation,

$$\sigma = \frac{Fs}{A} = \frac{wb \times w^2 \times R}{b \times h \times N}$$

$$\sigma = 3,32 \text{ MPa}$$

From the calculations above, the resulting voltage was on below of the maximum allowable stress design that was 27.57 MPa. It can be concluded that the size of the strut with a width x height of 60 x 12 mm it was safe to use.

5. Generator

Generators were used in the wind turbine design was a permanent magnet generator which is capable of producing 1000 watts at 450 rpm of rotation. These generators were imported from Ginlong Manufacturer, an electric generator factory, PMG types.

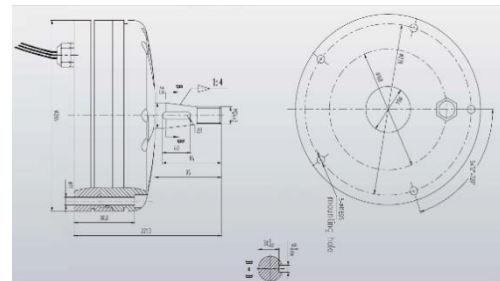


Figure 6. Generator GL-PMG-1000

Table 3 shows the specifications of generator GL-PMG-1000. It can be seen that the rated rotation speed of 450 rpm to produce a power output of 1000 watts.

Tabel 3. Spesifikasi GL-PMG-1000

Electrical Specification	
Rated Output Power(W):	1000
Rated Rotation Speed (RPM):	450
Recified DC Current at Rated Output (A):	6
Requied Torque at Rated Power:	31.5
Phase Resistance (Ohms):	12
Output Wire Square Section (mm ²):	4
Output Wire Length (mm):	600
Insulation:	H Class
Generator configuration:	3 Phase star connected AC output
Design Lifetime:	>20 years

6. Transmision

From Table 3, the generator rated rotation in order to produce an output power of 1 kW is 450 rpm while the axis wind turbines rotation only at 233 rpm. Therefore, it is necessary to raise the transmission shaft rotation. Transmission used was a bevel gear as shown in Figure 4:20.

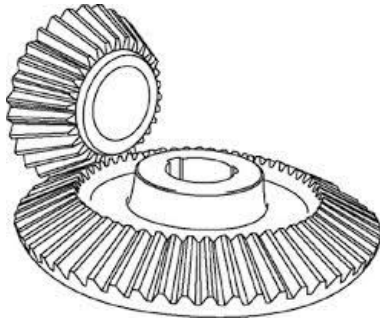


Figure 7. Bevel gear

Determining the size of the diameter of the gear (DG) and the diameter of the pinion (DP) using the equation, [8],

$$\frac{DG}{DP} = \frac{nP}{nG}$$

obtained DP = 100 mm dan DG = 200 mm.

7. Shaft

The main shaft will be reinforced using a hollow shaft which also will become a pillar of the wind turbine. In addition, this pillar also serves to put the taper bearing on the end of a pole. Calculation of shaft diameter of hybrid vertical axis wind turbine the axis type of the twisting moment (Te) and bending moment (Me).

a. From twisting moment (Te) maka,

$$Te = \frac{\pi}{16} \times \tau \left[\frac{(do)^4 - (di)^4}{do} \right]$$

b. From maximum normal tension (Me) so,

$$Me = \frac{\pi}{32} \times \sigma \left[\frac{(do)^4 - (di)^4}{do} \right]$$

Diameter was obtained in (on) and outer diameter (do) a maximum of hollow shafts are respectively 110 mm and 220 mm.

CONCLUSION

Based on the analysis and discussion of the H-rotor turbine 1kW design for coastal areas, Suwuk Kebumen, some conclusions can be drawn as follows:

1. The data processing speed of the wind result on the suwuk beach using Weibull distribution shows that wind speeds are frequent or frequent (VF) 4.37 m/s meanwhile the wind speed that can produce the maximum energy (VE) amounted to 7.99 m/s.
2. The result design of H-rotor wind turbines for the coastal areas is as follows suwuk:

H-Rotor

Airfoil Setion	NACA 0018
Jumlah Sudu	3
Solidity Ratio (σ)	0,24
Diameter Rotor (D_d)	2,7 m
Tinggi Rotor (H_d)	2,7 m
Panjang Chord (c)	0,216 m
Luas Sapuan (A)	7,29 m ²

Komponen Turbin

Diameter poros	90 mm
Panjang poros	9000 mm
Lebar dan tebal pasak	28 × 16 mm
Panjang pasak	15 mm
Diameterudukan strut	250 mm
Tebal dudukan strut	55 mm
Lebar strut	60 mm
Tebal strut	12 mm
Diameter luar bearing	140 mm
Diameter dalam bearing	90 mm
Tebal bantalan poros	21 mm
Tinggi tiang	8000 mm
Generator	Ginlong GL
Transmisi	PMG-1kW Bevel gear

REFERENCE

- [1] S., Eko, Baruna, Pusat data dan Informasi ESDM
- [2] Mathew, Sathyajith, *Wind Energy Fundamentals, Resource Analysis and Economics*. New York: Springer. 2006.
- [3] M.S., Hameed, A., Kamran, *Design And Analysis Of A Straight Bladed Vertical Axis Wind Turbine Blade Using Analytical And Numerical Techniques*. Journal of Ocean Engineering, Vol. 57, pp. 248-255. 2013.
- [4] J., Anderson, *Fundamental of Aerodynamics*. McGraw Hill Series in Aeronautical and Aerospace Engineering. 2010.
- [5] Koksai, *Self-Starting Darrieus Wind Turbine*. Design Project, MECH4020. Department of Mechanical Engineering Dalhousie University. 2004.
- [6] Koksai, *Vertical Axis Wind Turbine*. Design Project MECH4010. Department of Mechanical Engineering Dalhousie University. 2005.
- [7] R.W., Tresher, *Trend in Evolution of Wind Turbin Generator Configuration and Systems*. Journal of Wind Energy, Vol. 1, No. 1, pp. 70-86. 1998.
- [8] R.S., Khurmi, J. K., Guptha, *A Textbook of Machine Design*. New Delhi: Eurasia Publishing House (Pvt) Ltd. 2002.
- [9] K.R., Ajao, J.S.O., Adeniyi, *Comparison of Theoretical and Experimental Power output of Small 3-bladed Horizontal-axis Wind Turbine*. Journal of American Science, Vol. 5, No. 4. 2009.
- [10] Blackwell, *Wind Tunnel Performance Data for Darrieus Wind Turbine With NACA 0012 Blades*. Sandia Laboratory Energy Report. 1977.
- [11] Nurchayati, W., Kade, *Karakteristik Kincir Angin Tipe Wind Mill Berbahan Fiber Metal Laminate (Fml) Pada Variasi Kecepatan*

- Angin Dan Sudut Kemiringan Blade*. Jurnal Teknik Rekayasa, Vol. 10, No. 1, pp. 1-4. 2009.
- [12] S.O., Oyedepo, S.A., Muyiwa, S.P., Samuel, *Analysis of wind speed data and wind energy potential in three selected locations in south-east Nigeria*. Journal of Energy and Environmental Engineering, Vol. 3, No. 7. 2012.
- [13] M., Mulyadi, *Analisis Aerodinamika pada Sayap Pesawat Terbang dengan Menggunakan Software Berbasis Computational Fluid Dynamics (CFD)*. Depok: Universitas Gunadarma. 2010.
- [14] N., Tanti, A., Arnetto, *Pembuatan Program Perancangan Turbin Savonius Tipe-U Untuk Pembangkit Listrik Tenaga Angin*. Journal of Mechanical, Vol. 2, No. 1, pp. 1-5. 2011.
- [15] H., Arwoko, *Desain Turbin Angin*. Surabaya: Departemen MIPA UBAYA. 1999.
- [16] N., Mittal, *Investigation of Performance Characteristics of a Novel VAWT*. Thesis. UK: Departement of Mechanical Engineering University of Strathclyde. 2001.
- [17] J.F., Manwell, J.G., McGowan, A.L., Rogers, *Wind Energy Explained, Theory, Design an Application*. John Wiley and Son, Chichester. 2002.
- [18] Y., Daryanto, *Kajian Potensi Angin Untuk Pembangkit Listrik Tenaga Bayu*. Balai PPTAGG - UPT-LAGG. 2007.
- [19] P., Jain, *Wind Energy Engineering*. United States: The McGraw-Hill. 2011.
- [20] Islam, *Analysis Of The Design Parameters Related To A Fixed Pitch Straight-Bladed Vertical Axis Wind Turbine*. Journal of Wind Engineering, Vol. 32, No. 5, pp. 491–507. 2008.
- [21] M. R., Sidiq, *Pembuatan dan Pengujian Turbin Angin Darrieus dengan Diameter 30 cm dan Tinggi 30 cm*. Tugas Akhir Sarjana. Bandung: Teknik Penerbangan UNNUR. 2008.

BOVINE BONE HIDROKSIAPATITE MATERIALS MECHANICS PROPERTIES AT 900°C AND 1200°C OF CALCINATION TEMPERATURE

Antonius Adi Hendra Saputra¹, Joko Triyono², Teguh Triyono²

¹Program Studi Teknik Mesin – Universitas Sebelas Maret

²Staf Pengajar – Program Studi Teknik Mesin – Universitas Sebelas Maret

e-mail addresses : somedark17@gmail.com

Keywords:

Scaffold, BHA, Porous, Microvickers, Compressive Strength, SEM, Calcination

Abstract:

The aims of this study is to determine the mechanical characteristics of the calcinated scaffold material bovine hydroxyapatite (BHA) for bone filler applications. Scaffold BHA was obtained from femur section of bovine bones which cut into 10x10x10 mm. Scaffold BHA was calcinated by temperature variations of 900°C and 1200°C for 2 hours with 10°C/min as the amount of the increasing level. The study result of each scaffold BHA which had been calcinated by 900°C and 1200°C has a hardness value of 8.48 ± 0.1118 VHN and 12.37 ± 0.5803 , meanwhile the compressive strength value of each scaffold BHA samples is 3.03 ± 0.6764 MPa and 1.96 ± 0.3450 MPa. The porous on scaffold BHA samples calcinated by 900°C and 1200°C which had been observed by SEM had porous size that is not much different, it was ± 200 -400 μm , the difference can be seen from the smaller porous size of the scaffold BHA calcination 1200°C compared to the porous size of scaffold BHA calcination 900°C.

INTRODUCTION

Approximately 40% of body rigorous tissue damage due to brittle bones, bone cancer or accidents occurred in Indonesia, and the rest as congenital [1]. The bone filler needs for transplant and implantation were significantly increased on its restoration. An inexpensive bone filler material was necessary for Indonesian patients because there were fewer transplantation donors. Synthetic materials such as metal alloys or bioceramics were expensive because it is imported, whereas the cow bones waste as a bioceramics scaffolds raw material is abundant in Indonesia. Many studies were utilizing it to create hydroxyapatite material (HA) as one of the bioceramics products variants which used for the medical field that has economic value and environmental friendliness.

Hydroxyapatite (HA) is an excellent biomaterial for substituting bone because it has excellent biocompatibility. Hydroxylapatite or hydroxyapatite (HA) with $\text{Ca}_5(\text{PO}_4)_3(\text{OH})$ of molecular formula however, people often write as $\text{Ca}_{10}(\text{PO}_4)_6(\text{OH})_2$ is a calcium bioceramics apatite which can be found in human teeth and bones. It derived from natural sources which can form a strong bond to the bone tissue. Cow bone composition is consisting of 93% hydroxyapatite ($\text{Ca}_{10}(\text{PO}_4)_6(\text{OH})_2$) and 7% β -tricalcium phosphate ($\text{Ca}_3(\text{PO}_4)_2$, β -TCP) [2]. A porous HA became a fundamental requirement for the bone fractures or cracks reconstructions. The forming bones were served as a bone cells tissue structuring mediator that grows, which can increase bone regeneration properly [3].

HA itself is divided into two types: natural and synthetic. Natural hydroxyapatite is hydroxyapatite

which is produced by using natural ingredients that contain a rich of calcium of carbonate CaCO_3 . Calcium carbonate can be easily found in the environment around us, such as bones, shells, and malleable animal shields. Synthetic hydroxyapatite is hydroxyapatite which is made chemically. It is not only obtained by reacting synthetic compounds, but can also be achieved by reacting synthetic compounds with natural compounds. It is known as one of the important material because it has the bioactive, biocompatible, and osteoconductive properties which are similar to natural bone mineral, so it can be used as a human hard tissue substitution.

Bone filler is made from hydroxyapatite, hydroxyapatite can be made from bones, shells, and malleable animal shields. In health area, its orthopedic surgeon needs is a direct scaffold which utilized to fill the bone damage. Therefore, HA powder has to be further processed into a scaffold. This process requires high temperatures of about 1400°C, so it is costly. The metal plate applications can not be done because it could not be used as a bone filler. Due to, it will be taken back if the bones has been constructed.

Calcination on beef bones to turn it into hydroxyapatite is necessary. It was used to eliminate bacteria or agents which cause disease [4]. The higher calcination temperature was also very influential in cow bone hydroxyapatite crystallinity level [5]. Its intensity was increased significantly with the increasing of temperature and becomes more prominent as the temperature rises above 600°C. Hydroxyapatite calcination temperature has an optimum temperature to produce the best hydroxyapatite from various temperature calcination

levels. Its variations affect the cow bones mechanical properties. Therefore, it needs a temperature that can produce hydroxyapatite which had the best results. On several studies suggest that temperatures of 900°-1200°C had the best results. The best performance of the scaffold was 900°C. Its treatment was important to create a resilient scaffold HA [6]. The optimum temperature was 900°C for having formed crystals with a high degree of crystallinity or a perfect crystal [7]. Sintering temperature of 1200 ° C and 1300 ° C had higher results containing HA crystals, which have a high density and good mechanical properties [8]. HA was sintered at 1000°C, 1200°C, and 1300°C. Its hardness value increased as the sintering temperature, and maximum compressive strength values obtained on a sample of sintering temperature 1200°C [9]. HA which was generated in this study will be calcined by varying the calcination temperature, ie 900°C and 1200°C.

This study was conducted a preliminary study of scaffold bovine hydroxyapatite manufacture with cow bone waste raw material with calcination methods. Cow's femur was then cut to obtain the size of 10x10x10 mm. Cow bone calcination process was performed by 900°C and 1200°C of variations in temperature. HA calcination process was using 10°C of temperature rise every 1 minute until it reaches 900°C and 1200°C of temperature respectively. It was accomplished to determine the value and material properties of HA from bovine bones. This study results were expected to be purposed as a new biomaterials and bone filler for fractured patients.

RESEARCH METHODOLOGY

Initial assembling

The initial step in research was to set up the cow bone, thigh one (femur) was obtained from a slaughterhouse cattle/ slaughter house (RPH) in Jagalan street No. 26, Jagalan Village, District Jebres, Surakarta, Central Java Province with cow age range of 2-3 years. The bones were cleaned of meat and fat, then was boiling for 2 hours about 2-3 times until the existing oil at bone and fishy smell disappeared. Afterthat, it was carried out the drying bones to get bone dry, and it was cut using a bone saw machine to get shape/ size of 10x10x10 mm/pieces. The following process can clearly be seen on Figure 1.

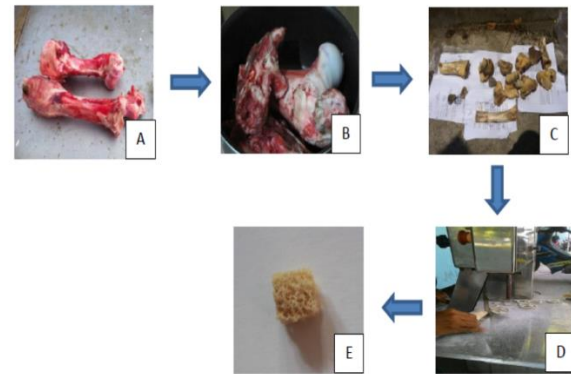


Figure 1. Execution Process

Annotation:

- (A) Raw bones
- (B) Boiling process
- (C) Drying process
- (D) Cutting process, 10x10x10 mm of size
- (E) Scaffold bovine 10x10x10 mm

Calcination process

The calcination process was performed to obtain a pure HA, calcination was executed by varying 900°C and 1200°C of temperature. HA calcination process was using 10°C of temperature rise every 1 minute until the temperature reaches 900°C then held for 2 hours and then cooled again to room temperature (27°C) and the same was operated at a temperature of 1200°C. The following Figure 2 shows a furnace.



Figure 2. Furnace

Testing

This study was implemented three tests, namely hardness, compressive strength test, and HA material characteristics. Hardness testing was using a Vickers Hardness Number (HVN) testing machine with 100g of load and pushing the indenter 10 seconds.

Compressive strength testing was operating by Universal Testing Machine (UTM) in accordance with ASTM standard F-451-95 using a Universal Testing Machine (JTM Technology Machine, 0.5T Capacity) with a load of 50 kg at a speed of suppression 5 mm / min.

SEM (Scanning Electron Microscopy) observations was using SEM (VEGA3 TESCAN) with 20.0 kV HV SEM, Low Vac 17 Pa, 31 Pa, and

15 Pa. It was conducted to determine the bones porous wall surface detail.

RESULT AND DISCUSSION

Calcination Temperature Effect to Bovine Bone Powder

Bovine bone was processed by 2 different calcination temperatures were 900°C and 1200°C. A calcined bovine bone from room temperature (27°C) up to temperatures of 900°C with an increase 10°C/min and then hold for 2 hours and cooled again to room temperature (27°C), the same method was performed on samples of cow bones calcined at a temperature of 1200°C. During the calcination process, the bone color has been changed between before and after calcined. After calcination, it has a white color and been become bovine hydroxyapatite (BHA). Bovine bone scaffold color, before calcination process at room temperature was yellowish white. The following figures portray bovine bone before and after the calcination process is shown in Figure 3.

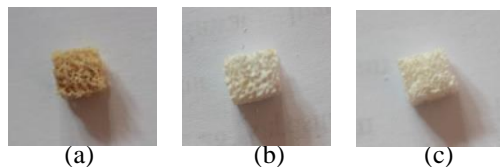


Figure 3. Bovine bone color: (a) Before calcined, (b) After calcined at 900°C, (c) After calcined at 1200°C.

Figure 3 displays the color change from white yellowish to white after calcination, it caused by the organic material decomposition. The white one was generated as a result of the organic material decomposition completely and obtained only the inorganic material.

This was reinforced by studies which claim that the calcination results at 400°C, 500°C, and 600°C of temperature, the bone samples color were turn black, dark gray, and light gray respectively. The calcined bone at $\geq 700^\circ\text{C}$ of temperature, it became white which was indicating the organic matter loss on the bone. This change was believed that linked to the organic matrix burning process (protein and collagen) in a bovine bone. The dark color of bovine bone samples under a temperature of 700 ° C were showed incomplete decomposition of organic material. The results were obtained from FTIR analysis showed that bovine bones gradually release OH⁻ ions at a temperature above 1100°C (Ooi et al, 2006).

Same as Ooi et al, (2006), Herliansyah et al, (2009) stated that the bovine bone which was containing large pores and small pores but generally a raw bovine bone microstructure was very dense because of their organic substance impregnated with inorganic minerals associated with it. After it has been heated at 900°C for 2 hours, microstructure was changed due to the water content evaporated (about 9 wt %) and organic substances such as collagen

(approximately 20 wt.%), proteins, polysaccharides, and lipids which were also contained in a small number, and only a hard inorganic part with high porosity was remaining. The XRD results showed that BHA at a temperature above 1000°C which indicates its decomposition, it decomposed and turned into tri-calcium phosphate (TCP).

[1] declared that the increasing of a bovine bone scaffold calcination temperature showed discoloration, and dark color indicates the incomplete decomposition of organic matter composition. At room temperature, a white bovine bone scaffold slightly yellowish, black at a temperature of 300°C, gray at a temperature of 600°C, 900°C, and white color 1, temperature and 1200°C.

The same was done by [10] that the increasing temperature of bovine bones calcination showed the same color product, HA at room temperature (before calcined) was white yellowish color, at temperature of 700°C, 900°C, and 1200°C were white. Dark gray color was occurred at 400°C of temperature and light gray color appeared at a temperature of 600 ° C, this happens due to the organic substances presence inside the bone. HA was decomposed to another calcium phosphates phase like tri-calcium phosphate (TCP) when calcined at temperatures over 1000°C, so that the calcination temperature played an important role in controlling the HA phase stability and mechanical properties.

From [11], [12], [1], and [10] explanation, it can be concluded that the color change from yellowish white to white after calcination due to the organic substances decomposition (protein and collagen).

Vickers Hardness Testing Analysis

From the data in Figure 4, hardness test results show that the hardness of scaffold BHA samples after calcination was increased. At calcination temperature of 1200°C was higher than 900°C of temperature. It portrays that the high temperature of calcination was affecting an increasing of bovine bone scaffold hardness. This could be happen due to the organic material disappearance on the bones surrounds, so bones became harder. Then, the highest hardness sample was chosen as the best sample which was BHA with calcination temperature of 1200°C with ± 0.5803 12:37 HVN.

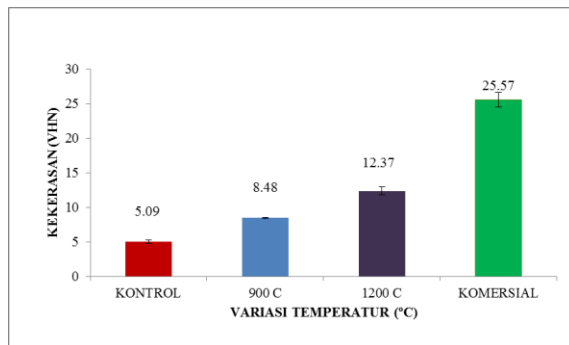


Figure 4. Microvickers scaffold BHA hardness.

It was stated by studies that claim that the HA hardness increases with the increasing of calcination temperature. HA hardness was increased from 152.2 MPa (15:52 VHN) at a temperature of 600°C, 172 MPa (17:54 VHN) at a temperature of 750°C, and then to 192 MPa (19:58 VHN) at 1000°C. [13]. From [13] explanation concluded that the effect of calcination temperature increasing generated the bovine bone material hardness. However, scaffold BHA hardness was exhibited still far from 25.57 ± 1.0692 VHN of commercial HA hardness.

Axial Compressive Strength Analysis

From Figure 5 can be clearly seen that compressive strength of the scaffold BHA specimens is decreased. At 900°C of calcination temperature, it produced 3.03 ± 0.6764 MPa of a compressive strength. At a temperature of 1200°C the compressive strength was decreased, compared to scaffolds BHA calcination temperature of 900°C which was 1.96 ± 0.3450 MPa. Scaffold BHA compressive strength test results portrays that bovine bone before calcined was produced higher compressive strength compared to BHA after calcined. The decreasing of compressive strength was provoked of the calcined bovine bones organic material disappearance, only produced inorganic materials that make BHA calcination becomes more porous. Hardness was inversely proportional to the compressive strength due to the samples hardness. Then, it was also more brittle than calcined sample with a lower hardness [9].

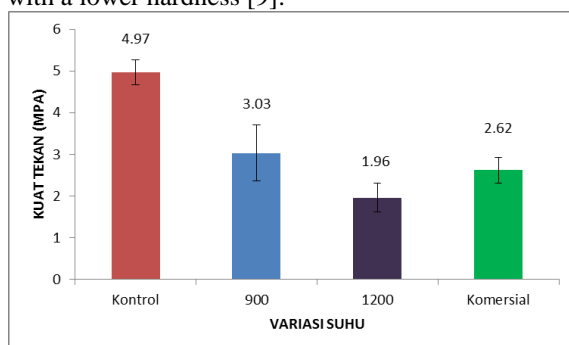


Figure 5. Axial Compressive Strength scaffold BHA testing result

It was reinforced by researches which declare that bovine bone before calcined showed highest compression and higher it has been calcined. The higher the calcination temperature provides lower compressive strength. The declining of compressive strength due to organic binder was reduced and porousnya bovine bone increased. The BHA strength with PVA coatings was higher than without coating. The PVA percentage expansion will enhance the BHA compressive strength [1]. From [1] explanation was achieved that its high temperature calcination can decrease the compressive strength rather than it has not been calcined. The commercial HA has higher compressive strength compared to the calcined BHA Scaffold at 900°C was 5.80 ± 0.9702 MPa, however the calcined BHA scaffold at 1200°C has a lower compressive strength.

Scanning Electron Microscopy (SEM) Scaffold Bovine Hydroxyapatite (BHA) Observation

Table 1 at 900 ° C illustrates the BHA porous scaffold interconnection. It can be recognized the interconnected porous in $\pm 200-400 \mu\text{m}$ sized picture. This calcination process removed an organic material and the remaining inorganic material, it was hydroxyapatite. Table 1 at 1200°C of temperature demonstrated the BHA porous scaffold interconnection with porous size that was not much different from 900°C was $\pm 200-400$. Its temperature of 1200°C has a size smaller its wall, which means the size of the porous getting bigger than its porous wall temperature of 900°C. Its growing porous size caused it became more brittle, thus decreasing the compressive strength.

Table 1. BHA scaffold micro structure after calcination of 900°C and 1200°C

Suhu Kalsinasi	Perbesaran 50x	Perbesaran 100x
900°C		
1200°C		

This was reinforced by studies which confirmed that the BHA scaffold calcination temperature of 900°C. It was demonstrated porous interconnections exhibit $\pm 200-300 \mu\text{m}$ of porous. Bovine bone material calcination can eliminate organic and inorganic residual materials were

hydroxyapatites. Calcination process also made it becomes more porous [1]. Similar to [1], [14] announced that 600°C of the calcination temperature, HA grain, and the tissue porous structure was not clearly visible, with the increasing calcination temperature of 750°C and 900°C, porous interconnected structure became quite noticeable. The constructed porous was very nice as bonding tissue when it purposed in ortopedi devices. [10] reported that it still looks collagen and proteins in bovine bone SEM results at 400-500°C of temperature. BHA SEM results at 600-1000°C of temperature to manufacture a special porous interconnection formations and the organic matter disappearance. From [1] and [14], [10] explanations can be concluded that the SEM result at 900°C and 1200°C of calcination temperature were seen an interconnection and BHA walls diminution porous occurred since temperature calcination was climbed up.

In scaffold bovine hydroxyapatite (BHA) research which has been given 900°C and 1200°C of calcination treatment temperature for 2 hours with a 10°C/ min of rising temperature. It has 12:37 ± 0.5803 HVN of hardness, 8:48 ± 0.1118 HVN of minimum requirement. The maximum compress strength was 3:03 ± 0.6764 MPa, minimum compressive strength was 1.96 ± 0.3450 MPa. SEM observations indicated that 200-400 μm of the porous interconnect size. Calcination temperature of 900°C was identified to be the best calcination temperature than the calcination temperature of 1200°C with 8:48 ± 0.1118 HVN of hardness and has 3:03 ± 0.6764 MPa of maximum compress strength.

CONCLUSION

In this study were obtained several conclusions as follows:

1. BHA scaffold hardness was increasing due to the calcination temperature. It produced 12:37 ± 0.5803 HVN at 1200°C which was higher than 8:48 ± 0.1118 VHN at 900°C of temperature.
2. Bovine bone before calcination had compress strength was higher than bovine bone that has been calcined ie 5419 ± 1.3758 MPa. The BHA scaffold compress strength at 900°C of a temperature 3.03 ± 0.6764 MPa which created higher than 1200°C BHA scaffold was 1.96 ± 0.3450 MPa.
3. SEM observations at 900°C and 1200°C of temperature presented an interconnection porous and produced ±200-400 μm of sized.

REFERENCE

[1] A.E., Tontowi, P., Dewo, E.T., Wahyuni, J., Triyono, *Scaffold Dari Bovine Hydroxyapatite Dengan Poly Vynialcohol Coating*, Jurnal Teknosains, Vol. 1 (2). 2012.

- [2] C., Ooi, M., Hamdi, S., Ramesh, *Properties of Hydroxyapatite Produced by Annealing of Bovine Bone*, Ceramics international, Vol. 33 (7), pp. 1171-1177. 2007.
- [3] F., Heidari, M., Razavi, M., Ghaedi, M., Forooghi, M., Tahriri, L., Tayebi, *Investigation of Mechanical Properties of Natural Hydroxyapatite Samples Prepared by Cold Isostatic Pressing Method*, Journal of Alloys and Compounds, Vol. 693 pp. 1150-1156. 2017.
- [4] A., Ruksudjarit, K., Pengpat, G., Rujijanagul, T., Tunkasiri, *Synthesis and Characterization of Nanocrystalline Hydroxyapatite from Natural Bovine Bone*, Current applied physics, Vol. 8 (3), pp. 270-272. 2008.
- [5] A., Niakan, S., Ramesh, P., Ganesan, C., Tan, J., Purbolaksono, H., Chandran, *Sintering Behaviour of Natural Porous Hydroxyapatite Derived from Bovine Bone*, Ceramics International, Vol. 41 (2), pp. 3024-3029. 2015.
- [6] A., Niakan, S., Ramesh, C., Tan, J., Purbolaksono, H., Chandran, W., Teng, *Effect of Annealing Treatment on the Characteristics of Bovine Bone*, Journal of Ceramic Processing Research, Vol. 16 (2), pp. 223-226. 2015.
- [7] Scalera, F., Gervaso, F., Sanosh, K., Sannino, A., and Licciulli, A., 2013, *Influence of the Calcination Temperature on Morphological and Mechanical Properties of Highly Porous Hydroxyapatite Scaffolds*, Ceramics International, Vol. 39 (5), pp. 4839-4846.
- [8] J., Triyono, S., Susmartini, E., Susilowati, S.A., Murdiyantara, *Shellac Coated Hydroxyapatite (Ha) Scaffold for Increasing Compression Strength*, Advanced Materials Research. 2015.
- [9] A., Handayani, *Preparation and characterization of Porous Hydroxyapatite from Fish Bone*, Jurnal Sains Materi Indonesia, Vol. 14 (1), 2012.

CU ADDITION EFFECT ANALYSIS ON MATRIX OF REMELTING PISTON ALUMINIUM COMPOSITE WITH SILICA SAND REINFORCEMENT TO THE IMPACT STRENGTH AND MICRO STRUCTURE ON ALUMINIUM MATRIX COMPOSITE USING STIR-CASTING METHOD

Fajar Paundra¹, Teguh Triyono², Wahyu Purwo Raharjo²

¹Mahasiswa Jurusan Teknik Mesin – Universitas Sebelas Maret

²Staf Pengajar – Jurusan Teknik Mesin – Universitas Sebelas Maret

e-mail addresses : fajarpaundra@gmail.com (Fajar Paundra)

Keywords :

Aluminium Matrix Composite, Stir casting, impact test, microscopy test,

Abstract :

AMC (Aluminium Matrix Composite) is material which has a great potential for being developed. This research was done to find effect added of Cu variation for impact strength and microstructure on Al-Si composite. Mass fractions of sand silica is 3% and Cu variation adding is 0, 1, 2, 3 & 4%. Composite manufacture is using stir casting method with stirring 600 rpm during of 5 minutes on semi solid temperature. Specimens were tested using optical microscope and impact charpy testing machine. The value impact of composite without adding Cu is 0,333 J/mm² after added Cu value down. Until adding Cu 4% the value impact is 0,104 J/mm². Micro photograph showed the result of porosity and SiO₂ unform distribution with the adding of Cu to the composite. From the test results it is known that the strength of the impact decreases with mass fraction addition Cu. This is because the addition of Cu can increase the porosity and formed CuAl₂ phase which are brittle.

PENDAHULUAN

In recent years, aluminium has been occupying an important role in the automotive, aircraft and construction industry. In the automotive field, the aluminum applications is in second place after steel. Due to its corrosion resistant properties, good thermal conductivity, and high strength-to-weight ratio, several automotive components are made of aluminum alloy, for instance, pistons, engine blocks, cylinder heads, valves, and so on. However, pure aluminum is not applied yet because it still has a poor casting and mechanical properties. Therefore, it is necessary to add other alloy elements to improve the mechanical properties on casting process. Alloy elements are often assembled, such as, copper (Cu), silicon (Si), magnesium (Mg), manganese (Mn), nickel (Ni), etc. [8].

In material development, a numerous research has been done to obtain an exact characteristic. Metal matrix composites (MMCs) are generally made by combining two or more ingredients, first ingredient is a base material (matrix) of light metals such as aluminum, while other material is a reinforcing material in particles form. It properties depends on several factors that influences them, such as, composite material type, reinforcement volume fraction, dimension, shape, and some other process variables.

Stir casting is a MMCs casting method in which materials are the combining of reinforcing material to a molten metal by stirring that makes the metal composites of uniform ceramic particles distribution

and reduces bubbles which is trapped in the molten metal.

An old piston is recycled into new pistons that have quality which equally expected to an original piston. The addition of Cu element into it which silica sand reinforced that contains of SiO₂ by stir casting methods is necessary to increase its strength. It is expected to have an equal strength than the new piston.

From the description above, it is necessary to do research about additional Cu variations on aluminum matrix composite of a used piston remelting with silica sand casting by stir casting method to its impact strength and micro structure. The purpose of this study was to determine the variations effect in copper (Cu) addition on impact strength, porosity, photos macro, and microstructure of silica sand reinforced aluminum matrix composites by stir casting method.

RESEARCH METHODOLOGY

The stir casting was used in this process which metal aluminium heated to melt at 700 °C in the induction furnace. Then, it was added a copper powder and stir until blended, silica sand mixing temperature was lowered to 650 °C (semi-solid) and ran for 5 minutes at 600 rpm of speed swivel, after that the temperature was raised to the pouring temperature at 725 °C and poured on a mold which impact test specimens shaped.

The impact, porosity, macro, and microstructure photograph test was done in this research. The impact test was intended to measure how much

energy that can be absorbed by a material until it fractures. This test used Charpy impact test apparatus using the ASTM E23. The impact test specimen formula:

$$E = W \cdot R (\cos \beta - \cos \beta')$$

From the formula above then obtained the formula to calculate the impact value:

$$I_s = HI = \frac{E}{A_0}$$

Where:

I_s = Impact [J/mm²]

E = Energy [Joule]

W = Pendulum weight [9,5 Kg]

R = Pendulum height [810 mm]

α = Initial deviation angle

β = Final deviation angle

A_0 = Area [mm²]

(Standar ASTM E 23)

After that, it was examined macro test to discover type of fault that occurred on the test specimen. Testing was conducted to determine the distribution of micro particles that occurred in the test specimen and the effect on impact strength.

Porosity testing was done by using the equation

$$P = \left(1 - \frac{\rho_s}{\rho_{th}}\right) \times 100\%$$

with:

P = Porosity percentage (%)

ρ_s = Density sample or actual density (gr/cm³)

ρ_{th} = Theoretical density (gr/cm³)

The microstructure testing was conducted by optical microscope test equipment. This test was aimed to find the variation perngaruh addition of Cu in the aluminum metal matrix composite.

RESULT AND DISCUSSION

1. Impact Strength

Figure 1 shows that the impact strength is decreased with the addition of Cu mass fraction. Al-Si composite without the addition of Cu has the 0.333 J/mm² of impact strength, after the addition of Cu at 1% decline becomes 0.227 J/mm², and continued to decreased until the addition of Cu at 4% it resulted 0.104 J/mm² of impact. According to research [6] which more and more Cu density in the composite, it produced impact strength value declining due to the porosity increasing.

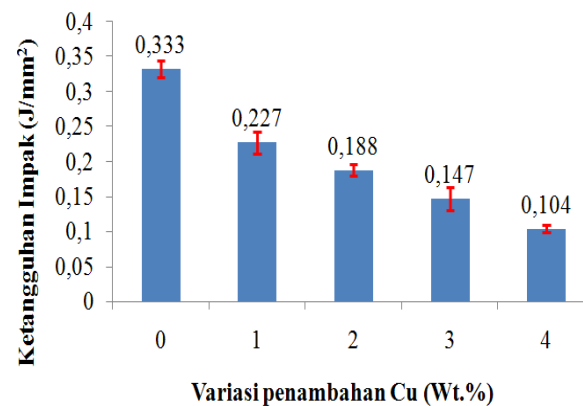


Figure 1 Impact testing result graph

2. Porosity Testing

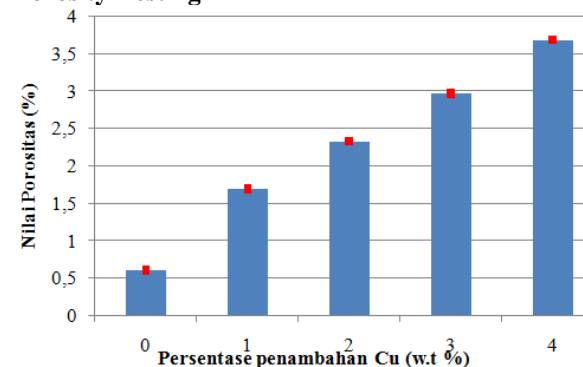


Figure 2 Porosity testing result graph

Figure 2 displays the porosity calculation results to 0%, 1%, 2%, 3%, and 4% of addition, where the porosity value is increased to the Cu addition. Cu has a negative effect on the porosity which more and more Cu is added to the composite Al-Si the more the porosity occurred. Copper was significantly increased the pressure of hydrogen gas causes the gas dissolved. On the Al-Si composite with copper addition was resulted in porosity which caused by gas increased, it is in line with the nature declining of the molten metal with increasing the percentage of Cu as stated by [3] and [11].

3. Macroscopic Photograph

The results on the cross-section of faulting macro image impact testing shows composite Al-Si mass fraction variation with the addition of copper has properties of ductile fracture, mix, and brittle.

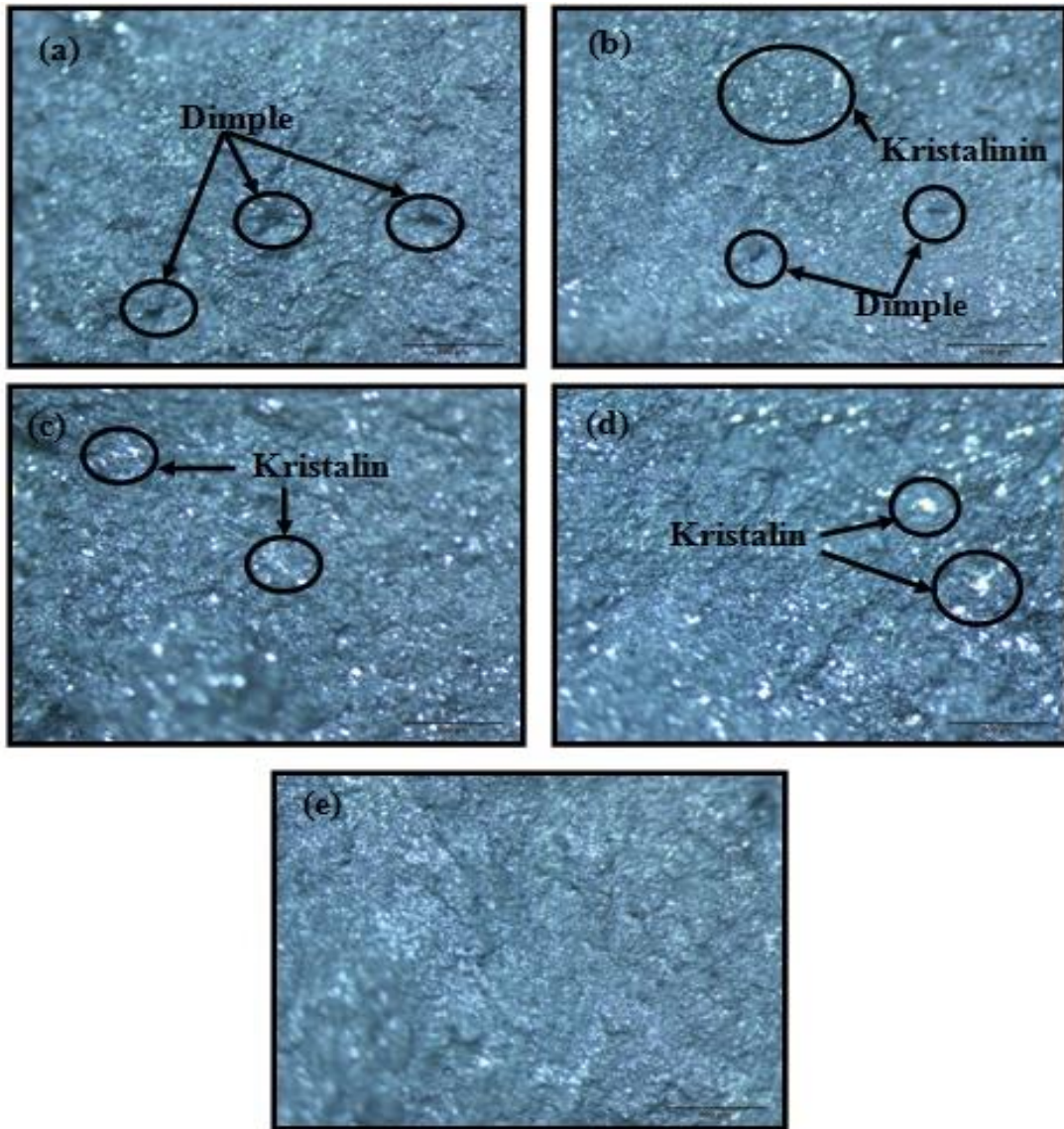


Figure 3 Macroscopic testing result (a) 0%, (b) 1%, (c) 2%, (d) 3%, and (e) 4% of Cu

Figure 3a portrays a composite Al-Si without Cu addition. Fracture surface is showed some dimples (the part that absorbs the light) that are large and slightly crystalline (the part that reflects light). It indicates the occurrence of plastic flow is large enough before fracture so it can be classified into ductile fracture. According to research which conducted by [7] of the fault analysis of impact on Al-Si composite which enforced by SiO₂ limits the plastic deformation that is absorbed by the matrix.

Figure 3b, 3c, 3d and 3e show a cross section of fracture composite with 1%, 2%, 3% and 4% of Cu mass fraction variations. Figure 3b, 3c and 3d display the mixed fracture (towards brittle), which is characterized by dimpel that began to decrease, crystals began to appear and growing. While Figure 3e is a composite Al-Si with the addition 4% of Cu mass fraction showed very brittle fracture, where it characterized by more flat fracture surface and more flat crystalline distributions. According to research conducted by [5] on the faults analysis on impact

charpy testing, where the fracture of brittle is produced from the grains cleavage mechanism of brittle metal, so when it exposed to external forces (impact), it exhibit a fracturing brittle which characterized by a flat fracture surface.

4. Micro Structure

Figure 4 shows the phase that formed on the Al-Si composites, such as aluminum (α) with the visible light colors, β form SiO₂ particles are grayish or dark, AlSi on the edge of SiO₂ and CuAl₂ elongated yellowish. According to research [4] and [12] on the aluminum microstructure analysis with the Cu addition, Figure 4 portrays the Cu adding effect on the SiO₂ distribution, where the composite without the Cu addition occurs the clumping of SiO₂ and after the addition the SiO₂ Cu is getting spread. It shows that the Cu addition on Al-Si composite serves as a wetting agent [9] where Cu can help the spread of particles reinforcement evenly. Copper aluminide (CuAl₂) is a phase that aluminum and

copper are cooled slowly from a single phase solid solution at room temperature [1] and [2]. CuAl_2 has very brittle properties and yellowish bright colored according to the study [13] on the analysis of micro structure AlSiCu with the Cu addition. CuAl_2 phase

in the composite AlSi was found on 2%-4% of Cu addition variation. Figure 4 also shows a porosity increasing where porosity is marked by the black dark and absorb light.

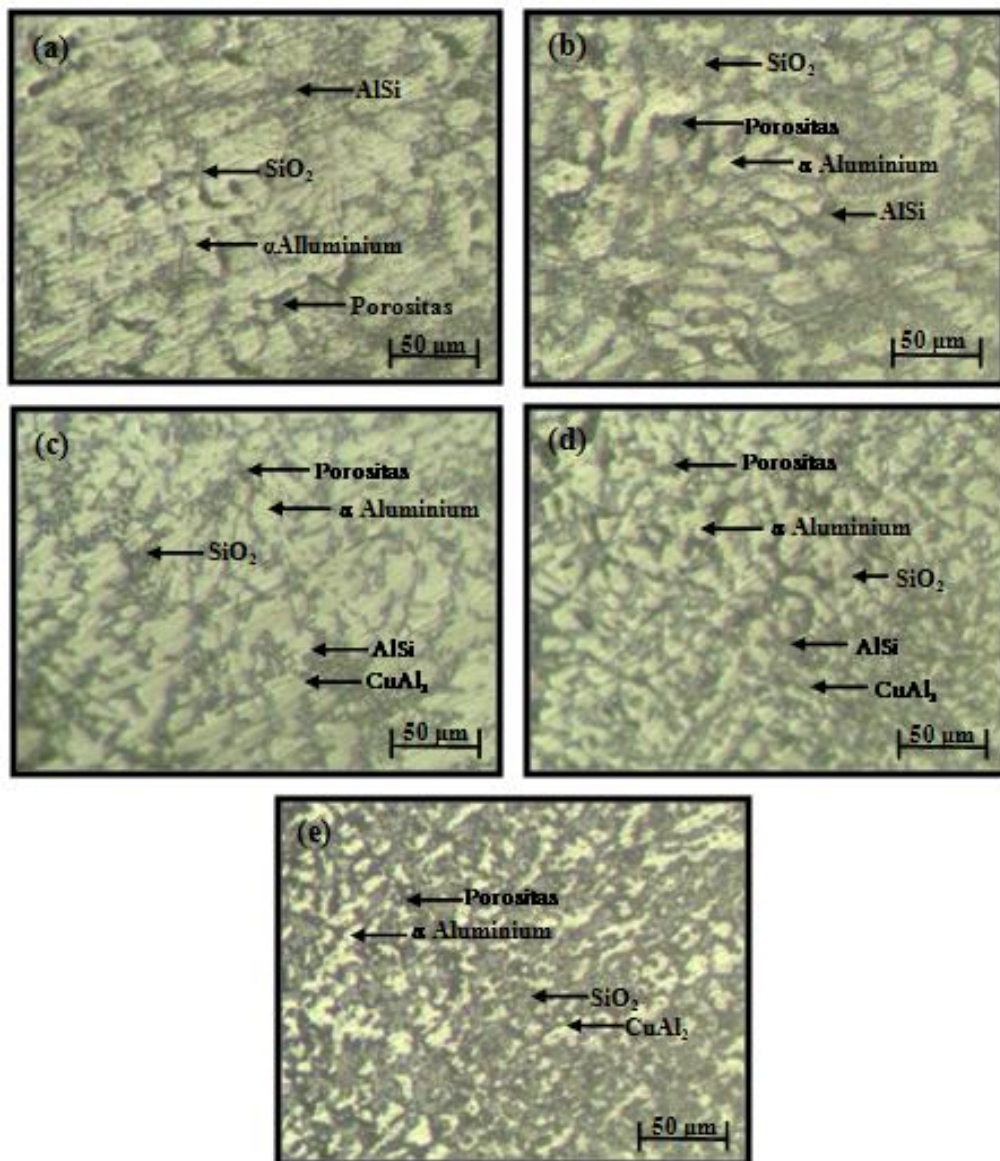


Figure 4 Composite Micro Structure (a)0%, (b)1%, (c)2%, (d)3%, and (e)4% of Cu

5. SEM Observation

Figure 5 displays the Al-Si composite without Cu addition. It shows the SiO_2 clots in certain areas, AlSi alloys found on the banks of SiO_2 . Figures 6 and 7 show the composite Al-Si with 2% and 4% of Cu mass fraction addition variations. Figures 6 and 7 show that SiO_2 is spreading and elongated shape with the addition of a mass fraction of Cu, this form

resulted in strength impaknya decreased, due to the form of SiO_2 tapered and elongated when exposed to external forces (impact) force will be centered at the ends so will be susceptible to fracture. This is according to research conducted by [10] on the characteristics of aluminum $\text{AC}_8\text{H}/\text{SiC}$ with stir casting process, in which the impact strength decreased due to the spread of the elongated SiO_2 .

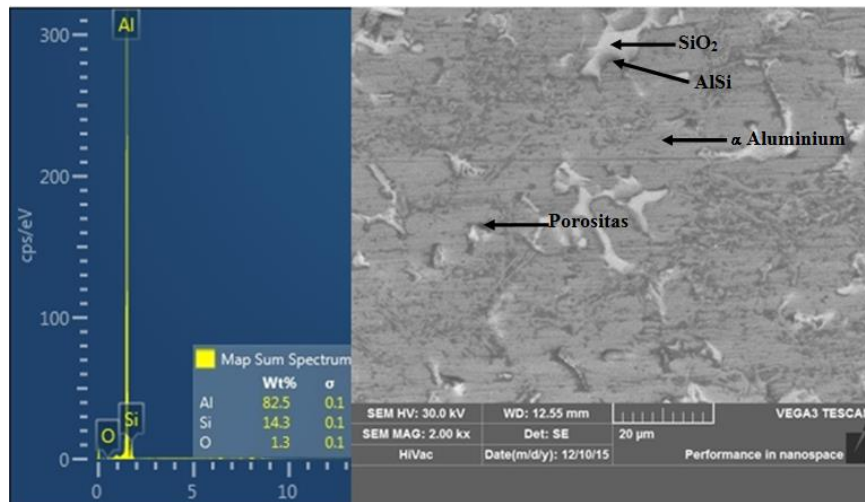


Figure 5 SEM testing result of composite without Cu addition

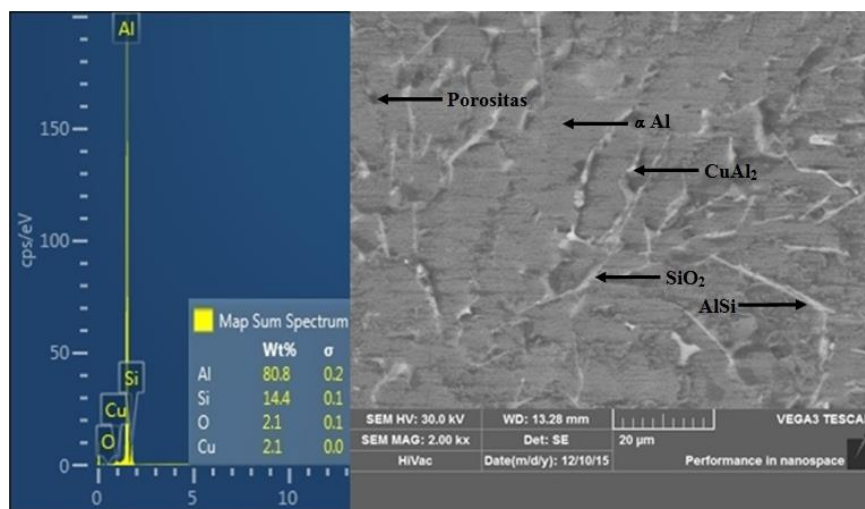


Figure 6 SEM testing result of composite with 2% of Cu

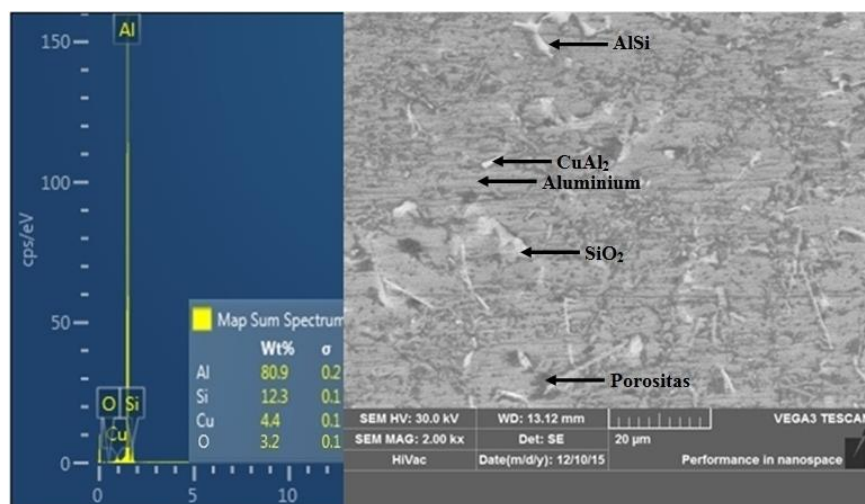


Figure 7 SEM testing result of composite with 4% of Cu

CONCLUSION

1. The composite impact strength was declined with Cu mass fraction. It can be seen from the porosity increasing calculation with Cu addition and macro image test results show a cross

section fracture impact test results experienced ductile fracture, mixture, and brittle.

2. The test results display that the microstructure and SEM SiO_2 which lengthen increasingly, tapered, and spreads along with Cu addition, due to its the mechanical properties tend to be weak

because if the material has a force from the outside, it will be centered on the ends of silicon, in addition to it also formed CuAl₂ phase which is brittle.

REFERENCES

- [1] M. F., Ashby, D. R. H., Jones, *Engineering Material 2*, Cambridge University, England. 1998.
- [2] G., Atmaja, *Analisa Sifat Mekanik Penambahan Unsur Cu pada Coran Aluminium*, Universitas Hasanudin, Makasar. 2011.
- [3] T.S., Deasy, Rusnaldy, Gunawan, *Pembuatan Bahan Standar AlSi12(b) Dari Skrap Aluminium Study Komposisi Kimia, Porositas dan Sifat Kekerasan Bahan*, Prosiding SNATIF, Universitas Diponegoro, Semarang. 2014.
- [4] A.N., Eva, *Analisa Sifat Fisis dan Mekanis Aluminium Paduan Al-Si-Cu Dengan Menggunakan Cetakan Pasir*, Universitas Muhammadiyah Surakarta, Surakarta. 2012.
- [5] Hasrin, *Analisa Perpatahan Baja ST 60 Yang Dikenai Beban Impak Charpy*, Politeknik Negeri Lhokseumawe, Aceh. 2013.
- [6] F.A., Hermawan, B.T., Sofyan, R., Rahmalia, *Studi Pengaruh Penambahan Cu Terhadap Karakteristik Komposit Al-8Zn-4Mg berpenguat SiC Hasil Squeeze Casting Untuk Aplikasi Balistik*, Fakultas Teknik Universitas Indonesia. 2013.
- [7] G.A., Kusumo, *Analisa Pengaruh Fraksi Massa Penguat SiO₂ Terhadap Kekuatan Impak Dan Struktur Mikro Pada Komposit Matrik Aluminium Menggunakan Metode Stir Casting*, Universitas Sebelas Maret, Surakarta. 2015.
- [8] R.S., Rana, R., Purohit, S., Das, *Reviews on the Influences of Alloying elements on the Microstructure and Mechanical Properties of Aluminum Alloys and Aluminum Alloy Composites*, Department of Mechanical Engineering, Maulana Azad National Institute of Technology, India. 2012.
- [9] A.A., Rizkiyani, *Pengaruh kadar Grafit Terhadap Karakteristik Komposit Aluminium Grafit Dengan Wetting Agent Tembaga*. Universitas Indonesia, Depok. 2008.
- [10] Y., Samuel, *Karakteristik Komposit Aluminium AC8H/SiC Dengan Proses Stir Casting*. Universitas Indonesia, Depok. 2012.
- [11] Subarmono, Janu, *Pengaruh Kadar Tembaga (Cu) Terhadap Sifat Fisis dan Mekanis Aluminium Matrix Composite Berpenguat Alumina Dibuat Secara Ekstrusi*, Prosiding, Universitas Gajah Mada, Yogyakarta. 2011.
- [12] Suherman, *Pengaruh Penambahan Cu Pada Paduan Al-7Si Terhadap Sifat Mekanis Dan Struktur Mikro Hasil Coran Kepala Silinder Motor 2 Tak Dengan Metode Pengecoran Lost Foam Casting*, Program Studi Teknik Mesin, Piliteknik Tanjungbalai, SUMUT, Vol.10, No. 1, Hal 10-13. 2014.
- [13] M., Zeren, K., Erdem, G., Serap, *Influence of Cu addition on microstructure and hardness near-eutectic Al-Si-xCu-alloys*, Kocaeli University, Kocaeli. 2011.

WELDING CURRENT AND SHIELDING GAS FLOW RATE EFFECT TO THE INTERMETALLIC LAYER FORMATION OF TUNGSTEN INERT GAS (TIG) ON DISSIMILAR METALS WELD JOINTS BETWEEN GALVANIZED STEEL AND ALUMINIUM AA 5052 BY USING Al-Si 4043 FILLER

Gilang Sigit Saputro¹, Triyono², Nurul Muhayat²

¹Mahasiswa Program Sarjana Jurusan Teknik Mesin – Universitas Sebelas Maret

²Staf Pengajar Jurusan Teknik Mesin – Universitas Sebelas Maret

Keywords :

*Tungsten Inert Gas welding
dissimilar metal
welding current
shielding gas flowrate
intermetallic
hardness*

Abstract :

Tungsten Inert Gas welding of galvanized steel-aluminium useful for weight reduction, improve perform and reduce cost production. The effect of welding parameters, welding current and shielding gas flow rate on the intermetallic formation and hardness of dissimilar metals weld joint between galvanized steel and aluminium by using AA 5052 filler was determined. In this research, welding speed was consistent kept. The welding parameters were obtained by using welding currents of 70, 80 and 90 A, shielding gas flow rate of 10, 12 and 14 litre/min. The intermetallic layer thickness increased by welding currents of 70 A to 80 A, but then it dropped on 90 A. The higher of a shielding gas flow rate, the lower the thickness of the intermetallic layer. The higher of a welding current, the lower the hardness of weld. The higher of a shielding gas flow rate, the greater the hardness of weld. As a result, the maximum hardness by current variation of 70 A and a shielding gas flow rate of 14 Litre/min was 100.9 HVN.

I. INTRODUCTION

Industrial development is rapidly growth, especially in automotive industry. Welding is widely used for the metal joining process, because it has some advantages such as strong joining, provident, cheap, and easy to apply. Many methods are used in metal welding processes. Tungsten Inert Gas (TIG) welding was selected in this study. The direct aluminum and galvanized steel welding is difficult to operate. It can be caused by a melting point big difference, thermal conductivity, incompatibility, and compound brittle intermetallic during the welding process [1].

Many studies are conducted to address these issues, such as aluminum alloys to low carbon steel with a filler metal of GTAW welding [2]. Fe-rich layer is separated from the surface during welding. Intermetallic layer has 15 μ m of thickness. The joining tensile strength was increased from 111 MPa to 150 MPa after a heat treatment. The aluminum to other galvanized steel joining experiments were using laser welding and GTAW welding [3]. Intermetallic layers, Fe-Al which fragile were easily formed under arc thus worsening the joining mechanical properties.

In this study was using TIG welding with protection argon gas and additional Al-Si 4043 as filler metal. It became necessary to find the most optimum variable in TIG welding process of galvanized steel to aluminum. Therefore, it could be reducing vehicle

weight, improving engine performance, and decreasing cost production [4].

II. BASIC THEORY

TIG welding is electric welding variety which are using tungsten materials as an unconsumed electrode. It serves only to conduct electricity from the power source to the essential metal. Therefore, it produces an electric arc flame which has a high thermal energy. Certain additives as filler rod was disbursed by the weld region filling arc flame. Noble gases such as argon, helium, and CO₂ are used as a protective gas to prevent oxidation from outside air to the liquid metal which being welded.

TIG welding is suitable for thin plate welding because it has a limited heat input. The filler metal feeding rate does not depend on the welding current. TIG welding process is very clean which can be used for the reactive metals such as titanium, zirconium, aluminum, and magnesium. Electrical currents which are too high can cause tungsten electrode melting and generate a welding brittle inclusions. The welding process uses a tungsten electrode which is not an added ingredient. Electric arc that occurs between the end of the tungsten electrode and the base material is a welding heat source. Figure 2.1 shows the TIG welding process when fusing and connecting the metal by heating it through an arc which formed from a tungsten electrode that is not consumed by the primary metal.

Its torch grip is connected to the protector gas tube as in Figure 2.1 (a). It is usually contacted to copper tube cooling water, called a contact tube as shown in Figure 2.1 (b), which is attached to the terminal welding cable. The welding electric current is flowing from the power source to the electrode and it is cooled to prevent excessive heat. Workpiece is associated to the other terminal on the power source through a different cable 2. Shielding gas enters through the torch body. It is aimed by the nozzle toward the weld pool to protect the entry air from outside environment. The GTAW welding air protection is better than GMAW from its inert gas which directly targeted to the weld pool. For this reason, GTAW welding is also referred to TIG welding.

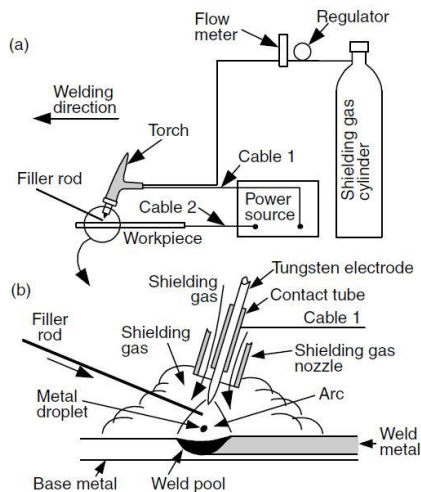


Figure. 2.1 Tungsten Inert Gas Welding, (a) whole process; (b) welding area [5].

III. RESEARCH METHODOLOGY

III.1 Equipment dan Materials

TIG welding machine in Figure 3.1 (a) which was used, it has 5-200 A of output current and 85% of efficiency. JIG was practiced as in Figure 3.1 (b) with such designed which is able to clamp the workpiece perfectly. Therefore, the connection density can be maintained.



Figure 3.1 (a) TIG Welding Machine dan (b) JIG Plate Clamp

The materials which operated as the parent metal was 200 x 80 x 3 mm of aluminum plate AA 5052 and 200 x 80 x 1.2 mm of galvanized steel, while Al-Si 4043 wire shaped of filler metal with 1.6 mm of diameter as shown in Figure 3.2 was also performed. Pure tungsten with 2.6 mm of diameter was employ which not consumed during the welding process.

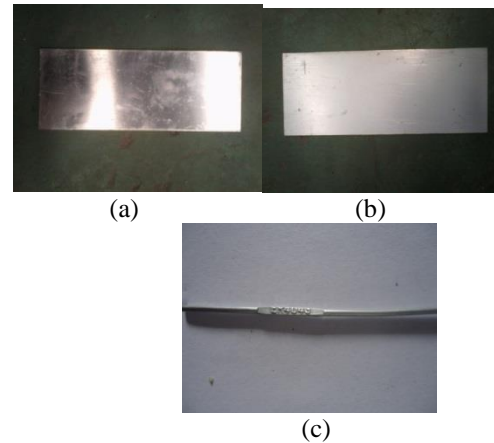


Figure 3.2 Aluminium AA 5052 as Main Metal (a), Galvanised Metal (b), dan (c) Al-Si 4043 filler.

Chemistry composition for each material is shown on Table 3.1 and Table 3.2.

Table 3.1 Chemistry composition base metal

Type material	% C	% Mg	% Cr	% Al	% Si	% Cu	% Fe	% Zn
Baja Galvanis	0.050	3.0	-	0.6	0,019	-	Bal	-
Aluminium A5052	-	2.2-2.8	0.15	95.7	0.25	0.10	0.40	0.10

Table 3.2 Chemistry composition filler metal Al-Si 4043 [6]

Weight%	Al	Si	Fe	Cu	Ti	Zn	Mn	Mg	Others
Alloy 4043	Bal	4.5-6.0	0.80 max	0.30 max	0.20 max	0.10 max	0.05 max	0.05 max	0.05 max each

III.2 Research Methodology Scheme

Figure 3.3 shows a research method flowchart. The independent variables that used in this study was 70 A, 80 A, 90 A of electric current and 10 L/ min, 12 L/ min, 14 L/ min of shielding gas flow rate. The dependent variable was the intermetallic layer formation and the hardness number from the TIG welding process on galvanized steel and AA 5052 of aluminum. Controlled variable was welding speed.

Determining the research scope which is preferred therefore determined boundary problem as follows:

1. A constant welding speed of 60 mm/ min.
2. Cleaning the surface of the plate is uniformly performed using alcohol.

3. Cooling welds performed in air at room temperature.

Welding process was performed by an experienced welder and has been certified by a recognized training weld institution that can ensure a uniform filet form on the outcome of the welds so it will not affect the test results in this study.

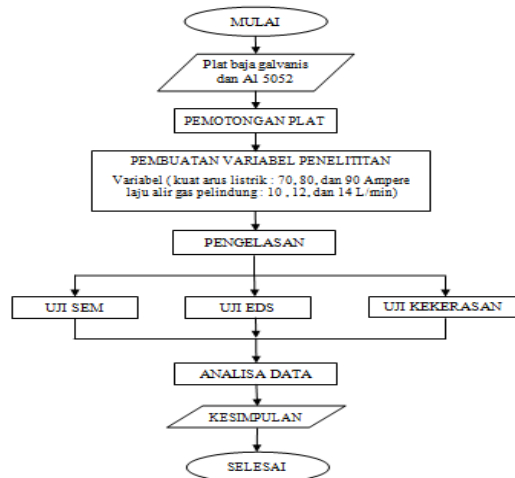


Figure 3.3. Research method flowchart

AWS D1.1 / D1.1M: 2006 was as a standard geometry for plate preparation as shown in Figure 3.4. A5052 aluminum alloy plate and galvanized steel 200 x 80 x 1.2 mm of dimensions and 25 mm of length of overlap welding connection.

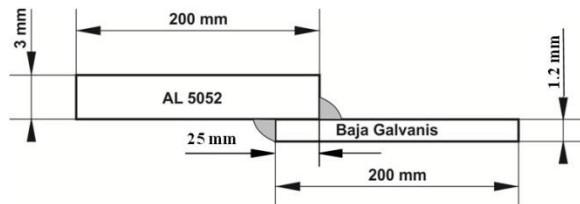


Figure 3.4 Lap joint plate configuration based on AWS D1.1/D1.1M:2006

III.3 Testing

Layer formation testing was using a scanning electron microscope (SEM) and energy dispersive spectrometry (EDS), while hardness was using Vickers testing machine. SEM and EDS preparation, a welding specimen which has been connected was cut in the middle and then filed until flat. Specimens that have been refined and then polished using autosol to remove residual sanding scratches. Then, the specimens were etched with modified reagent poulton in aluminum with 6 grams CrO_3 of mixture composition, 15 ml of HCl , HNO_3 , and 1.25 ml of HF which mixture by 21.25 ml of distilled water. Etsa fluid for low carbon steel galvanized using a composition mixture 1 ml of HNO_3 which blended in 10 ml of distilled water. SEM

and EDS testing areas scheme is shown in Figure 3.5. Vickers testing was conducted to determine the hardness distribution in aluminum base metal, heat affected zone (HAZ), and the aluminum weld using 200 gf for 10 s of loading. Vickers hardness test scheme is shown in Figure 3.6 :

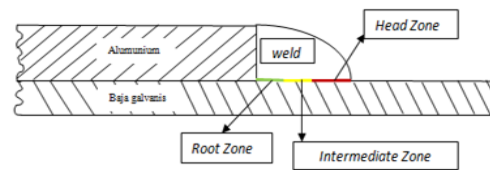


Figure 3.5. SEM dan EDS testing area [7]

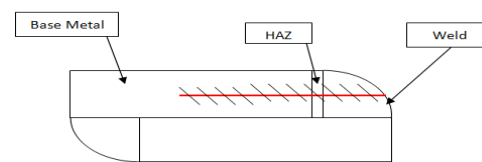


Figure 3.6. Vickers hardness testing scheme [8]

IV. DATA ANALYSIS

IV.1.1 Intermetallic layer on Head Zone

There are 3 weld sections were tested by SEM such as, head zone, intermediate zone, and root zone. Head zone is free layer reaction part which was indicating the liquid weld on galvanized parts. At the galvanized coating head zone of steel has been destroyed and several dendrites begin to grow from the interface and there was a micro-pore shrinkage in the inter dendrites. At the intermetallic, there are 4 important atomic constituents are Fe, Al, Si, and Zn. On EDS testing was taken from 7 spectrums vertically from the welds, intermetallic layer to galvanized. For all variations, the number of atomic Fe was increased while Al was declined, while the Si atoms and Zn values were uncertain.

Figure 4.1 shows the test results on the SEM head zone for all variations. Intermetallic layer thickness will be increased from 70 A to 80 A of current and will decrease to 90 A. Si content was determining the thickness or thinness of intermetallic layer. The greater content of Si atoms will make the grain size becomes small and prevents diffusion of Fe atoms from the base metal galvanized steel, thereby reducing the thickness of the intermetallic layer and increase its tensile strength [9].

Figure 4.2 displays EDS testing result in all variations. At 70 A of current, 0.6% of Si, and then declined to 0.2%. of Si content was less cause intermetallic layer that forms were becoming increasingly bold. Intermetallic layer on 90 A of current becomes thinner. It could be caused by the

increasing 3.2% of Si content. On 12 liters/ minute of protected gas flow rate, 0.3, 0.1, and 3.5% of Si content and 14 liter/ min of gas flow hedge rate: 1.1, 0.4 and 0.9%.

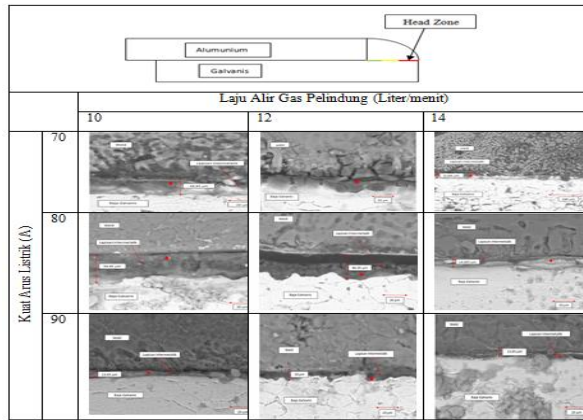


Figure 4.1. Head zone testing result

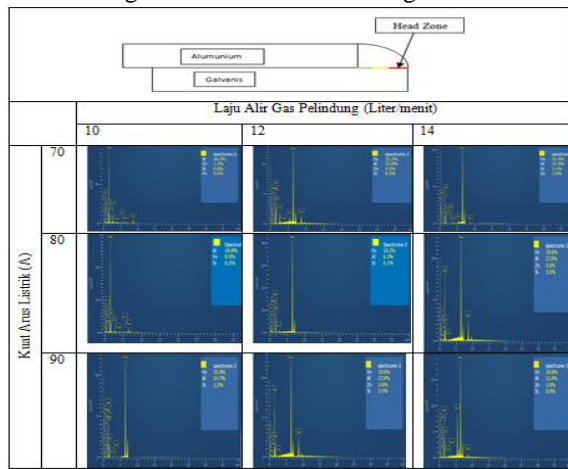


Figure 4.2. EDS testing result on head zone

Intermediate zone is part of the reaction layer with a thickness of at most. Reaction layer was formed by columnar crystals variable composition of Al and Fe. Intermetallic compounds configuration was consisting of two phases, namely $FeAl_3$ at the aluminum and galvanized Fe_2Al_5 in the nearby area [10]. Figure 4.3 shows SEM testing result at the intermediate zone for all variations. At 80 A of current by an additional thickness of the intermetallic layer thickness then decreased in 90 A of current. In 80 A of current heat input becomes larger therefore the cooling rate widened more slowly, causing the formation of $FeAl_3$ be increased and the size becomes larger [10]. The increasing current will stimulate the thickness of the reaction layer in which the thickness of the layer decreases discontinuous reaction [11]. At 80 A of current was the peak of reaction layer. Therefore, 90 A of current reaction layer thickness will be decreased.

Figure 4.4 portrays EDS testing result at the intermediate zone for all variations. The content of 70

A of current at 1.0%, was down to 0.3% on 80 A of current and 90 A rise of current to 2.1% of the gas flow. The content 70 A of current: 0.3%, was down to 0.2% on 80 A and 90 A of current with 3.4% of Si content. Si content which was decreased at 80 A of current and an increased in 90 A of current proves that the increasing thickness of the intermetallic layer on 80 A of current and decreased thickness of the intermetallic layer on 90 A of current.

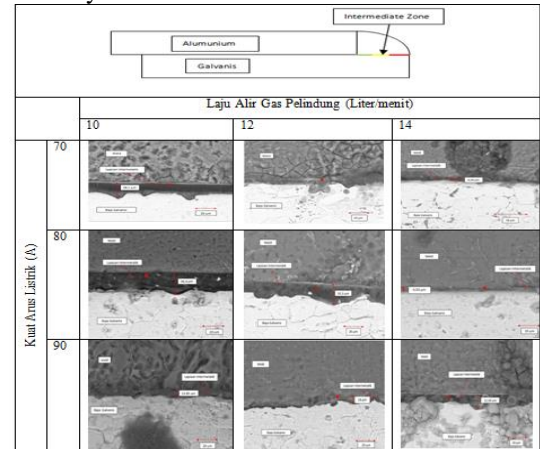


Figure 4.3 SEM testing results on Intermediate Zone

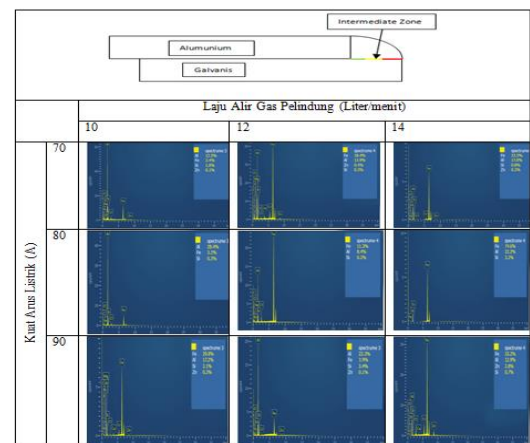


Figure 4.4 EDS testing result on Intermediate Zone

Root zone is the most complex which located between the steel and light strip where most contain zinc. From Figure 4.5 comparison, it can be seen that the greater the gas flow rate hedge for the same current, the thickness of the intermetallic layer will also be dwindling. According to the hypothesis, this is due to the same current, the greater the gas hedge rate the more gas that protects the weld from that will improve cooling rate and refine the grain size so the intermetallic layer was formed to be thinner. A deviation was occurred from the thickness of the intermetallic layer on 10 liters/ min of gas flow rate

decreased in the 12 liters/ min of gas flow rate and increased thickness in 14 liters/ minute of gas flow rate. Figure 4.6 EDS testing result on 90 A of current shows aberration reasons that Si content in the intermetallic layer. Si content in 10 liter/ min of gas flow rate hedging at 0.2% increased to 1.4% in 12 liter/ minute of gas flow rate hedging. The increasing of Si content caused the intermetallic layer becomes thinner. Si content decreased to 0.5% for 14 liter/ minute of gas flow rate hedging, so the intermetallic layer the thickness increased.

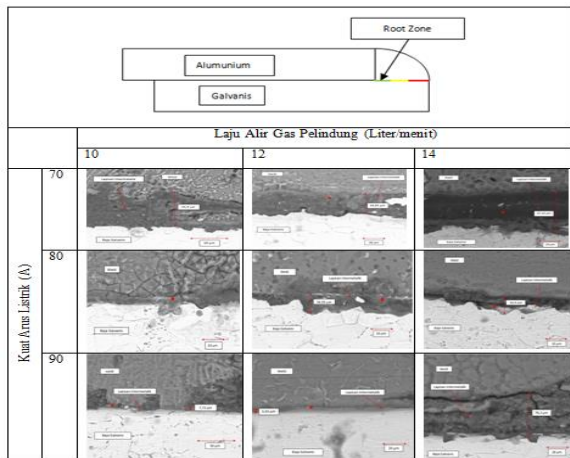


Figure 4.5 SEM testing result on root zone

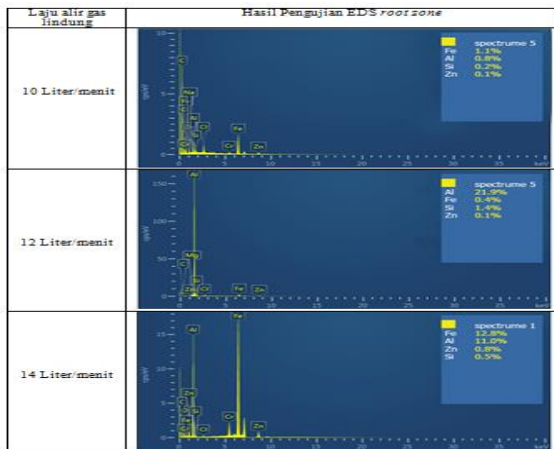


Figure 4.6. EDS testing result on root zone at 90 A of current

4.2 Vickers Hardness Testing Results

The electrical current addition is always directly proportional to the main voltage. This is in accordance with the laws of joules, increasing the electric current will also increase heat input and will cause the cooling rate (cooling rate) becomes slow. The greater the heat input will increase the size and spacing between the dendrite, which will lower the hardness [12]. It can be seen from the research results to increase the current with the same gas flow rate as shown in Figure 4.7.,

Figure 4.8., and Figure 4.9. For 10 liters/ minute of gas flow rate, the hardness average value at the weld decreased from 78.32 HV, 79.2 HV, and 72.58 HV. For 12 liters/ minute of gas flow rate, 92.02 HV, 82.5HV, and 80.54 HV, for a gas flow rate of 14 liters/ min of gas flow rate, 94.6 HV, HV 87.32, 83.8 HV were obtained. Protected gas at 10 liters/ minute of irregularities flow rate which the average weld hardness increased from 78.32 HV to 79.2 HV, due to the its content the 10 liters/ min of gas flow rate at 80 A of current was higher than 10 liters/ min of gas flow rate hedging at 70 A of current, the larger the content of Silicon, the grain size and the distance between the grains become smaller [9]. Therefore, the damage was also increased. The content of silicon in the weld test was known from EDS as shown in Figure 4.10 and Figure 4.11.

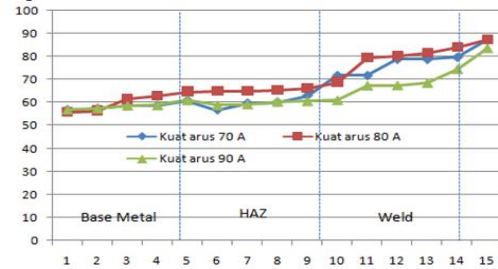


Figure 4.7 Vickers testing graph on 10 L/min

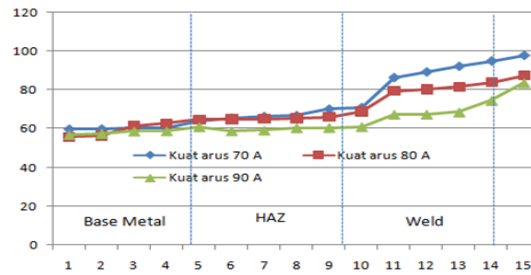


Figure 4.8 Vickers testing graph on 12 L/min

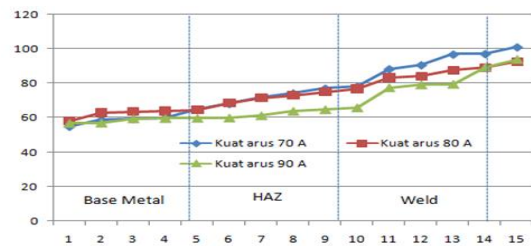


Figure 4.9 Vickers testing graph on 14 L/min



Figure 4.10 EDS testing result on 70 A, 10 L/min

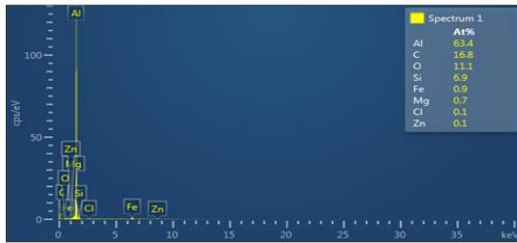


Figure 4.11 EDS testing result on 80 A, 10 L/min

Figure 4.7, Figure 4.8, and Figure 4.9 show an the increasing trend of ranging damage from aluminum base metal, aluminum heat affected zone, and welding. The highest hardness value was located in welding area due to hard of brittle intermetallic phase formation in the welding area [13]. Hard of brittle intermetallic phase as FeAl₃ and Fe₂Al₅ will also increase hardness and lower tensile strength

The shielding gas flow rate is a parameter that indicates the number of protected gas flowing in units of liters in one minute during the welding process. The greater the shielding gas, the greater the gas to protect the weld from adverse atmospheric air. From Figure 4.12, Figure 4.13, and Figure 4.14, it can be seen that the shielding gas flow rate affect the hardness value of welding area. The greater the gas flow rate will increase hardness values as shown in Figure 4.12 average hardness weld on 70 A of current: 78.32 HV, 92.02 HV, and 94.6 HV. Figure 4.13 shows the welding average hardness on 80 A of current: 79.2 HV, 82.5 HV, and 87.32 HV. Average weld damage at 90 A of current is shown by Figure 4.14: 72.58 HV, 80.54 HV, and HV 83.8.

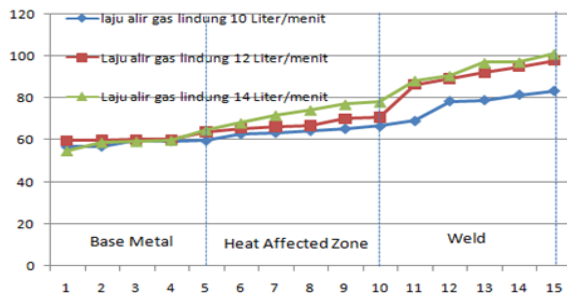


Figure 4.12. Vickers hardness testing graph on 70 A

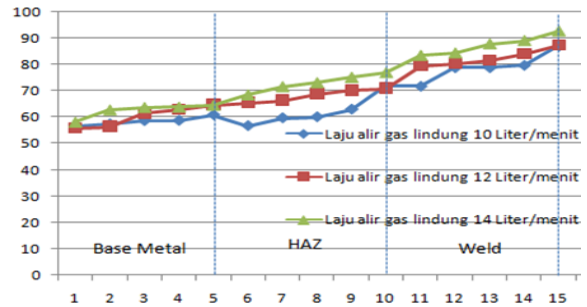


Figure 4.13. Vickers hardness testing graph on 80 A

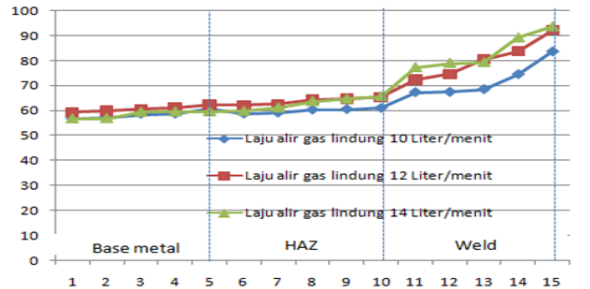


Figure 4.14. Vickers hardness testing graph on 90 A

V. CONCLUSION

- 1) The thickness of the intermetallic layer was increased from 70 A to 80 A of current variations, then fell on 90 A of current. The greater the shielding gas flow rate, the thickness of the intermetallic layer will fall.
- 2) The increasing electric current, the hardness will be decreased. Increasingly the protective gas flow rate will increase damage. The highest hardness variations occurred in 70 A of current and 14 L/ min of shielding gas flow rate with 100.9 HV of hardness.

VI. SUGGESTION

Authors recommend for the next researcher to conduct research on the analysis of the influence of the type of shielding gas and filler metal variations of the mechanical properties of TIG welded joints and steel aluminium.

VII. REFERENCE

- [1]
- [2] H., Dong, H., Wenjin, *Detachment of Interfacial Layers During Arc-Brazing of Aluminium Alloy to Carbon Steel with Filler Wire*. 2012.
- [3] G., Sierra P., Peyre , F., Deschaux-Beaume, D., Stuart, G., Fras, *Steel to aluminum key-hole laser welding*. Mater Sci Eng A 2007;447:197–208.
- [4] E., Schubert, M., Klassen, I., Zerner, C., Walz, G. L., Sepold, *Weight structures produced by laser beam joining for future applications in automobile and aerospace industry*. JMaterProcessTechnol2001;115:2–8. 2001.

- [5] K., Sindou, *Welding Metallurgy Second Edition*. 2003.
- [6] S. B., Lin, J. L., Song, *Dissimilar Metal TIG Welding-Brazing of Alumunium Alloy to Galvanized Steel*. 2009.
- [7] A., Mathieu, S., Rajasekar, *Dissimilar Material Joining Using Laser (Alumunium to Steel Using Zinc-Based Filler Wire)*. 2005.
- [8] H., Fatih, *The Effect of Welding Current on Heat Input, Nugget Geometry, and the Mechanical and Fractural Properties of Resistance Spot Welding on Mg/Al Dissimilar Materials*. 2010.
- [9] D., Honggang, H., Wenjin, *Dismilar Metal Joining Of Alumunium Alloy to Galvanized Steel with Al-Si, Si-Cu, Al-Si-Cu and Zn-Al Filler Wired*. 2011.
- [10] L., shao, Y., Shi. *Effect of joining parameters of dissmilar metal joints between alumunium and galvanized steel*. 2014.
- [11] Q., Rangfeng, S., Hongxin, *Interfacial of Joint Between Mild Steel and Alumunium Alloy Welded by Resistance Spot Welding*. 2010.
- [12] S., Gurjinder, K., Sunil, *Influece Of Current On Microstructur and Hardness of Butt Welding Alumunium AA 6082 Using GTAW Process*. 2013.
- [13] G., Qiang, W., Kehong, *Formation and Distribution Mechanism of Intermetallic Compounds Of Al/Mg Joint with Zn Transitional Metal*. 2010.

MANUSCRIPT WRITING GUIDELINES

Manuscript Writing Systematics

The writing sequences are as follows: title, author, and colleagues also affiliation and place of work, abstract, keyword, main article (Introduction, Research Methodology, Results, and Discussion, Conclusion), acclamation, reference, and appendix (if any). Abstracts, keywords, and content are written in English. Each abstract should not be more than 200 words. Abstract content is the subject, summary, and the conclusion of the article therefore it becomes an important document for information systems. The number of keywords is 2 to 10.

Manuscript Format

The manuscript should be typed on A-4 size of A-4 HVS paper, TNR size 10 in one column format. Margin is 2.5 cm, (top, bottom, left, and right). All pages must be numbered in sequence. The author is expected to give his writings in hard copy above the HVS A-4 as well as in the CD-R (using Ms. Word). The writing format on the CD should be the same as the hard copy. Submission of text and correspondence via electronic mail is preferred.

Equations and Units

The equations must be numbered. The serial number of the equation should be placed in parenthesis. All equations numbers must be placed on the right side of the equation and must be placed between the text. The unit used in the article is the SI unit. If other units should be used, then SI units should also be included in parenthesis. There are no special rules in the use of symbols or abbreviations, but it is recommended to use commonly used symbols. Symbols and mathematical formulas must be typed. Some symbols that provide doubt should be specified. Must be distinguished between the numbers one (1) and the letter l or I and between the numbers zero (0) and the letter o.

Pictures and Tables

Photos, graphs, illustrations or diagrams are included in the "Picture" group. All images and tables should be placed between the text and identified with the Latin letter (not Roman), are numbered according to the sequence (Sorting of different numbers between Figures and Tables). All letter sizes, line lengths or symbols must be uniform in black print on white and should be free of irrelevant information. All images must be clear and can be easily reduced to 50% of their original size. The typing should be clear and still read properly with 50% reduction. All tables and images must be accompanied by an explanatory legend.

Reference

The reference should be written down at the end of the article with enough information so readers can easily find it. Reference which is listed only related directly to the contents of the manuscript. Writing order : author name, year, title, publisher, and city of publication. Author name puts a family name or a reversed name, without a title. The reference literature quotes used are expressed by writing the author's name and the year published in parenthesis, for example: (Celata et al, 2000).

Associate Editor

All articles will be judged by an associate editor and will be sent back to the author along with the comments is given within one month from the date of collection. The editorial team will decide on the selection of the manuscript to be published after receiving the assessment results of the expert editing team. The editorial team is authorized to accept or reject the submitted manuscript, or to request the author to correct the manuscript. The author may provide a rebuttal to the comments/ suggestions provided by the associate editor.

Content writing is not the responsibility of the editor. All matters concerning licensing, use of computer software, script originality and other matters related to ownership and legal consequences may be the responsibility of the author. The Editor reserves the right to edit its editorial without altering the meaning and no correspondence unless the postal stamp will be returned (as it does not meet the requirements or needs to be corrected).

Each submitted manuscript shall be given a proof of loading and printing number each 3 (three) Copies. Additional requested copies or prepaid prints must be paid at special rates.